



1 **Marine Carbohydrates in Arctic Aerosol Particles and Fog – Diversity**
2 **of Oceanic Sources and Atmospheric Transformations**

3

4 **Sebastian Zeppenfeld¹, Manuela van Pinxteren¹, Markus Hartmann², Moritz Zeising³, Astrid**
5 **Bracher^{3,4}, and Hartmut Herrmann¹**

6

7 1 Atmospheric Chemistry Department (ACD), Leibniz-Institute for Tropospheric Research (TROPOS),
8 Leipzig, Germany

9 2 Atmospheric Microphysics (AMP), Leibniz-Institute for Tropospheric Research (TROPOS), Leipzig,
10 Germany

11 3 Alfred-Wegener-Institute Helmholtz Centre for Polar and Marine Research, Bremerhaven, Germany

12 4 Institute of Environmental Physics, University of Bremen, Bremen, Germany

13

14 **Correspondence to:* Hartmut Herrmann (herrmann@tropos.de)

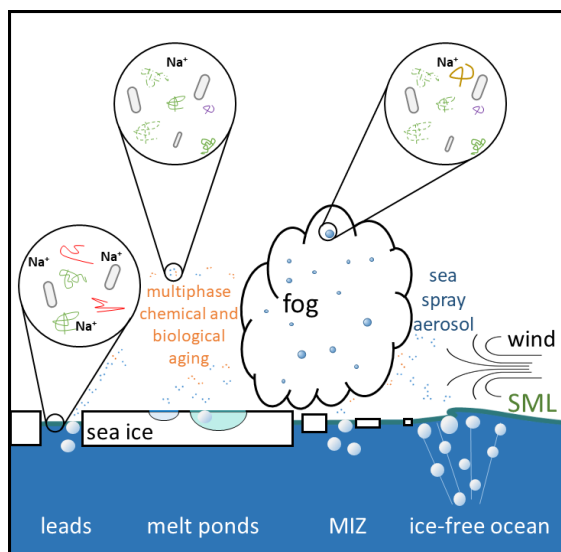
15

16

17

18 **Abstract**

19 We present the results of a ship-based field study about the sea-air transfer of marine combined
20 carbohydrates (CCHO) from concerted measurements of the bulk seawater, the sea surface microlayer
21 (SML), aerosol particles and fog. In seawater, CCHO ranged between 22–1070 $\mu\text{g L}^{-1}$ with large
22 differences among the different sea-ice related sea surface compartments: ice-free ocean, marginal
23 ice zone (MIZ), open leads/polynyas within the pack ice and melt ponds. Enrichment factors in the SML
24 relative to the bulk water were very variable in the dissolved ($\text{EF}_{\text{SML,dCCHO}}$: 0.4–16) and particulate
25 ($\text{EF}_{\text{SML,pCCHO}}$: 0.4–49) phases with highest values in the MIZ and aged melt ponds. In the atmosphere,
26 CCHO appeared in super- and submicron aerosol particles ($\text{CCHO}_{\text{aer,super}}$: 0.07–2.1 ng m^{-3} ;
27 $\text{CCHO}_{\text{aer,sub}}$: 0.26–4.4 ng m^{-3}) and fog water ($\text{CCHO}_{\text{fog,liquid}}$: 18–22000 $\mu\text{g L}^{-1}$;
28 $\text{CCHO}_{\text{fog,atmos}}$: 3–4300 ng m^{-3}). The enrichment factors for the sea-air transfer were calculated for
29 super- and submicron aerosol particles and fog, however strongly varied depending on which of the
30 sea-ice related sea surface compartments was assumed as the oceanic emission source. Finally, we
31 observed a quick atmospheric aging of CCHO after their emission with indications for both
32 biological/enzymatic processes (based on very selective changes within the monosaccharide
33 compositions of CCHO) and abiotic degradation (based on the depolymerization of long-chained CCHO
34 to short free monosaccharides). All in all, the present study highlights the diversity of marine emission
35 sources in the Arctic Ocean and atmospheric processes influencing the chemical composition of
36 aerosol particles and fog.



TOC Figure



38 1. Introduction

39 Sea spray aerosol (SSA) is one of the major aerosol species in the lower troposphere over the remote
40 Arctic Ocean, particularly during the boreal spring and summer months (Chi et al., 2015; Hara et al.,
41 2003). Depending on the size distribution and chemical composition, SSA strongly contributes to the
42 populations of cloud condensation nuclei (CCN) and ice nucleating particles (INP) affecting the polar
43 radiative budget through the formation of liquid droplets and ice crystals in fog and clouds (DeMott et
44 al., 2016; Lawler et al., 2021; McCluskey et al., 2018; Penner et al., 2001; Schiffer et al., 2018; Wilbourn
45 et al., 2020). Notably in the Arctic, one of the regions most affected by global warming, there is still a
46 lack of knowledge about the relationship between the formation and evolution of clouds and specific
47 chemical properties of primary marine aerosol particles (Wendisch et al., 2023).

48 SSA is emitted directly from the ocean surface through wind-driven processes and, as a consequence,
49 contains the salts and the organic matter (OM) present in seawater, including carbohydrates (CHO) as
50 one of the largest identified organic fractions (Quinn et al., 2015 and references therein). In
51 microalgae, bacteria and also more complex marine organisms (e.g. kelp, krill), carbohydrates have
52 important metabolic, structural and protective functions or are released in response to environmental
53 stress, such as freezing or lack of nutrients (Krembs et al., 2002; Krembs and Deming, 2008; McCarthy
54 et al., 1996; Mühlenbruch et al., 2018; Suzuki and Suzuki, 2013; Wietz et al., 2015). In seawater, the
55 majority of carbohydrates appears as linear or branched oligo- and polysaccharides, commonly
56 referred to as combined carbohydrates (CCHO), both in the dissolved (*d*CCHO) and the particulate
57 (*p*CCHO) phases. These macromolecules consist of several monosaccharides, such as hexoses,
58 pentoses, deoxy sugars, amino sugars, uronic acids and amino sugar acids, which are connected via
59 glycosidic bonds (Benner and Kaiser, 2003; Engel and Händel, 2011; Panagiotopoulos and Sempéré,
60 2005). Most CCHO are quite stable within the marine environment unless they are either hydrolyzed
61 in the presence of specific enzymes or in a very acidic setting (Arnosti, 2000; Panagiotopoulos and
62 Sempéré, 2005). Heterotrophic bacteria use extracellular enzymes to selectively degrade CCHO into
63 absorbable shorter molecules leaving a certain part as recalcitrant, more persistent OM (Alderkamp et
64 al., 2007; Becker et al., 2020; Goldberg et al., 2011; Wietz et al., 2015). While *p*CCHO is mostly
65 attributed to recent productions by local phytoplankton indicated by high positive correlations with
66 total chlorophyll *a* (TChl-*a*), *d*CCHO appears to be the result of more complex metabolic and
67 transformation processes after its release (Becker et al., 2020; Fabiano et al., 1993; Goldberg et al.,
68 2011; Zeppenfeld et al., 2021a). In contrast, dissolved free carbohydrates (*d*FCHO), short sugars in their
69 monomer form, are quickly consumed by marine microorganisms resulting in much lower
70 concentrations of *d*FCHO compared to CCHO in ambient seawater (Engbrodt, 2001; Engel and Händel,
71 2011; Ittekkot et al., 1981; Zeppenfeld et al., 2020).



72 In the remote marine atmosphere, carbohydrates are assumed to significantly impact cloud properties
73 by contributing to both the CCN and INP populations (Leck et al., 2013; Orellana et al., 2011; van
74 Pinxteren et al., 2022). Carbohydrates appear both in super- and submicron SSA particles (Aller et al.,
75 2017; Leck et al., 2013; Russell et al., 2010; Zeppenfeld et al., 2021a), most likely resulting from their
76 emission from the surface of the ocean after bubble bursting as part of jet and film droplets (Veron,
77 2015; Wang et al., 2017). In addition to the bulk surface seawater, the sea surface microlayer (SML) as
78 the uppermost layer of the oceanic water column is an important source of OM, and thus marine
79 carbohydrates, in the SSA. The SML is described as a gelatinous film on top of the ocean, which is often
80 enriched in surface-active substances or buoyant gel particles compared to the underlying bulk water
81 (Engel et al., 2017; Wurl et al., 2009, 2011; Zäncker et al., 2017). Entrained air bubbles rise within the
82 upper part of the water column, scavenges surface-active organics from the surface bulk seawater and
83 pass the thin SML. Eventually they burst there releasing film and jet droplets containing a mixture of
84 substances found within the bulk and the SML (Burrows et al., 2014). At the same time, surfactants,
85 exopolymers and microgels in the SML increase the stability of the cap films of the bubbles, extend
86 their lifetimes and enable the drainage of water-soluble compounds (Bigg and Leck, 2008; Bikerman,
87 2013; Sellegri et al., 2006). Consequently, the sea-air transfer occurs in a chemo-selective manner
88 leading to a strong size-dependent enrichment of surface-active organics relative to water-soluble
89 sodium (Na^+) and, hence, a relative chemical composition of SSA different to the surface seawater
90 (Facchini et al., 2008; O'Dowd et al., 2004; van Pinxteren et al., 2017; Prather et al., 2013; Quinn et al.,
91 2015; Triesch et al., 2021a, b). These chemo-selective enrichments of organic substances in the SSA
92 relative to bulk water, especially in the submicron size range, usually exceed the enrichments in the
93 SML by orders of magnitude (van Pinxteren et al., 2017; Schmitt-Kopplin et al., 2012). The underlying
94 mechanisms for the chemo-selective sea-air transfer of carbohydrates, including co-adsorption, are
95 complex and subject of several recent and ongoing laboratory tank and modelling studies (Burrows et
96 al., 2016; Hasenecz et al., 2020; Schill et al., 2018; Xu et al., 2023). After their emission, fresh SSA
97 particles, including the contained carbohydrates, undergo atmospheric aging due to a not yet well-
98 understood interplay of several atmospheric processes, such as atmospheric acidification, abiotic
99 radical chemistry and biological and enzymatic modifications (Angle et al., 2021; Hasenecz et al., 2020;
100 Malfatti et al., 2019; Trueblood et al., 2019; Zeppenfeld et al., 2021a), potentially also altering their
101 microphysical properties.

102 Besides SSA, high concentrations of marine carbohydrates in fog and low-level clouds in the marine
103 environment are plausible due to the high hygroscopicity of SSA serving as good CCN (Xu et al., 2022)
104 transferring OM from the particle into the liquid phase, the high water-solubility of carbohydrates and
105 cloud-borne microorganisms potentially forming carbohydrates in-situ (Matulová et al., 2014). Only a
106 few studies conducted at field sites exposed to marine air masses measured certain subgroups of



107 carbohydrates, such as primary saccharides (Dominutti et al., 2022) or transparent exopolymer
108 particles (TEP) (Orellana et al., 2011; van Pinxteren et al., 2022) so far in fog/clouds. However, the
109 sources of marine carbohydrates in marine ambient fog/clouds, including $dFCHO_{fog}$ and $CCHO_{fog}$, and
110 their relationship to the bulk seawater, SML and aerosol particles still lack elucidation.

111 During the summer months, the chemical compounds of natural SSA and marine fog can be studied in
112 the Arctic Ocean due to the low influence of long-range transported anthropogenic pollution (Bozem
113 et al., 2019; Schmale et al., 2021). However, the presence and seasonal evolution of Arctic sea ice
114 divides this pristine region into a complex ensemble of several sea-ice related sea surface
115 compartments. These encompass the open leads - sea ice fractures with variable widths of several
116 meters - and polynyas within the pack ice. Furthermore, there is the ice-free ocean, the marginal ice
117 zone (MIZ) defined via a sea ice concentration threshold between 15 and 80% (Rolph et al., 2020), and
118 melt ponds forming and developing during the melting season on top of the ice floes. These
119 environments are characterized by different chemical, physical and biological characteristics
120 potentially influencing the quantity and properties of the SSA emitted. Recent studies observed, for
121 instance, that the number and efficiency of Arctic INP are strongly dominated by the type of sea-ice
122 related sea surface compartments that the air masses had passed before sampling (Creamean et al.,
123 2022; Hartmann et al., 2021; Papakonstantinou-Presvelou et al., 2022; Porter et al., 2022). However,
124 the individual conclusions still appear controversial and might be biased by seasonal and interannual
125 variabilities. Consequently, more systematic studies in the Arctic, also with regard to the chemical
126 properties of the aerosol particles, are required to achieve more conclusive results.

127 To increase the knowledge about marine carbohydrates as important constituents of SSA and potential
128 CCN and INP, we present here the results of a comprehensive field study conducted onboard the
129 German icebreaker RV *Polarstern* from May to July 2017. We performed concerted measurements of
130 bulk seawater, SML, size-resolved aerosol particles and fog water at different locations dominated by
131 different sea-ice related sea surface compartments (ice-free, leads/polynyas, MIZ, melt ponds) in the
132 Arctic Ocean. All marine and atmospheric compartments are discussed and compared on absolute
133 CCHO concentrations, calculated $CCHO/Na^+$ ratios, the relative monosaccharide contribution to CCHO
134 and the occurrence of $dFCHO$. Eventually, we disclose the complexity of the primary emission
135 mechanisms and subsequent atmospheric aging of marine CCHO in the Arctic Ocean.



136 2. Experimental

137 2.1 Study area and field sampling

138 Field samples were gathered during the PS106 (PASCAL/SiPCA) campaign (Macke and Flores, 2018;
139 Wendisch et al., 2018) conducted from May to July 2017 in the Fram Strait, Barents Sea and central
140 Arctic Ocean including an ice floe camp period (05–14 June 2017) on board the German icebreaker RV
141 *Polarstern*.

142 Marine SML and corresponding bulk water samples were collected at various locations ([Figure SI 1](#))
143 from the ice-free ocean (four sampling events), open leads and polynyas within the pack ice (20
144 sampling events), young and aged melt ponds (six sampling events) and the MIZ (five sampling events).
145 SML samples were obtained by immersing a glass plate (length: 50 cm, width: 20 cm, thickness: 0.5 cm,
146 sampling area: 2000 cm²) vertically into the surface water and slowly withdrawing it at a speed of
147 approximately 15 cm s⁻¹ (van Pinxteren et al., 2012; Zeppenfeld et al., 2021a). The adhered SML film
148 was drawn off the glass plate surface into a prewashed wide-neck plastic bottle by a framed Teflon
149 wiper. The average thickness of the SML collected during this field study was 76±10 µm. The
150 corresponding bulk water was taken from a defined depth of 1 m into LDPE bottles attached to a
151 telescopic rod, except at the closed melt ponds where it was scooped from the bottom at
152 approximately 20–40 cm depth. Before each sampling, the sampling containers were first rinsed with
153 a few milliliters of the corresponding aqueous sample which was disposed immediately after. On
154 board, small aliquots of the water samples were analyzed immediately for salinity using a conductivity
155 meter (pH/Cond 3320, WTW), colored dissolved organic matter (CDOM) and particulate absorption
156 (PAB), with more details in section 2.6. For later chemical analyses (inorganic ions, pH, carbohydrates)
157 500–1000 ml of 0.2 µm filtered water sample, 0.2 µm polycarbonate filters and field blanks were
158 stored at -20°C.

159 The sampling of ambient aerosol particles was conducted at the starboard side of RV *Polarstern* at the
160 top of the observation deck at a height of approx. 25 m above sea level as already described in Kecorius
161 et al. (2019). Size-segregated aerosol particles were sampled in five size ranges (stage 1: 0.05–0.14 µm,
162 stage 2: 0.14–0.42 µm, stage 3: 0.42–1.2 µm, stage 4: 1.2–3.5 µm, stage 5: 3.5–10 µm aerodynamic
163 particle diameter with a 50% cut-off) on aluminum foils by using two synchronized low-pressure Berner
164 impactors (Hauke, Austria) with a flow rate of 75 L min⁻¹ and a sampling time of three to six days. To
165 avoid the condensation of atmospheric water and subsequent microbial activities on the aluminum
166 foils, a 3 m long heated tubes between the isokinetic inlets and the impactors reduced the relative
167 humidity of the sampled air to 75–80%, when the ambient relative humidity was higher. During this
168 field study, the difference of the temperatures of the ambient air at the inlet and the sampled air after



169 the heating never exceeded 9 K. Consequently, losses of semi-volatile compounds or changes by heat-
170 induced chemical reactions are expected to be neglectable. Furthermore, the Berner impactors were
171 thermally insulated by a polystyrene shell. After sampling, the foils were stored in aluminum containers
172 at -20°C until analysis. In this study, the results from stages 1-3, 4-5 and 1-5 were summed up as
173 submicron (sub), supermicron (super) and PM₁₀, respectively. Details about the size-resolved aerosol
174 particle samples and corresponding meteorological information are given in [Table SI 1](#), in total 15
175 complete sets of Berner foils).

176 Close to the aerosol sampling, fog was collected using the Caltech Active Strand Cloud Collector Version
177 2 (CASCC2) as described by Demoz et al. (1996). Bulk fog droplets were impacted on Teflon strands
178 with a diameter of 508 µm and collected into a prewashed Nalgene polyethylene bottle. The flow rate
179 was 5.3 m³ min and the 50% lower cut-off was determined to be approximately 3.5 µm. Further
180 information about the 22 fog samples collected during the PS106 campaign including meteorological
181 information can be found in [Table SI 2](#) and in Hartmann et al. (2021).

182 **2.2 Total aerosol particle mass concentrations**

183 Before and after sampling, the aluminum foils were equilibrated (three days, 20°C, 50% relative
184 humidity) and weighed using a precise microbalance (Mettler Toledo XP2U, weighing error: ±4.6 µg).
185 Total particle mass concentrations ($mass_{aer, stage\ y}$) were calculated for each Berner stage as the ratio
186 between the difference of the absolute foil masses after and before sampling and the sampled air
187 volume. Afterwards, aluminum foils were divided for further chemical analyses.

188 **2.3 OC/EC in aerosol samples**

189 Organic carbon (OC_{aer}) and elemental carbon on Berner aerosol foils were determined as described by
190 Müller et al. (2010) using a two-step thermographic method (C/S MAX, Seifert Laborgeräte, Germany)
191 with a nondispersive infrared sensor.

192 **2.4 Carbohydrates in aerosol particles, fog, seawater and melt ponds**

193 Marine carbohydrates in the particulate ($pCCHO$, >0.2 µm) and dissolved ($dCCHO/dFCHO$, <0.2 µm)
194 including truly dissolved molecules and small colloids were quantified from seawater and melt pond
195 samples following the protocol presented by Zeppenfeld et al. (2020, 2021a) using high-performance
196 anion-exchange chromatography with pulsed amperometric detection (HPAEC-PAD) equipped with a
197 Dionex CarboPac PA20 analytical column (3 mm × 150 mm) and a Dionex CarboPac PA20 guard column
198 (3 mm × 30 mm). The monosaccharides fucose (Fuc), rhamnose (Rha), arabinose (Ara), galactose (Gal),
199 glucose (Glc), xylose (Xyl), mannose (Man), fructose (Fru), galactosamine (GalN), glucosamine (GlcN),
200 muramic acid (MurAc), galacturonic acid (GalAc), and glucuronic acid (GlcAc) were identified by their



201 retention times. *dFCHO* represent the sum of identifiable monosaccharides before, and *dCCHO* and
202 *pCCHO* additionally released after an acid hydrolysis (0.8 M HCl, 100°C, 20 h). *CCHO* is the sum of
203 *dCCHO* and *pCCHO*. *CHO* represents the sum of *CCHO* and *dFCHO*, and consequently encompasses all
204 carbohydrates measured within this study. **Figure 1** gives an overview of the here used carbohydrate-
205 related abbreviations. Marine carbohydrates in fog water and extracts from size-resolved aerosol
206 particles were measured with (*CCHO_{fog}*, *CCHO_{aer}*) or without (*dFCHO_{fog}*, *dFCHO_{aer}*) prior acid hydrolysis.

207

208

209

210

211

212

213

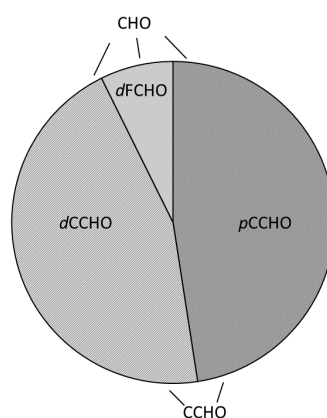


Figure 1. Overview of the abbreviations for carbohydrates (*CHO*) in seawater. *CCHO*: combined carbohydrates; *pCCHO*: particulate combined carbohydrates, *dCCHO*: dissolved combined carbohydrates; *dFCHO*: dissolved free carbohydrates.

214 **2.5 Sodium and pH in aerosol particles, fog, seawater and melt ponds**

215 Major inorganic ions, including sodium (Na^+), were determined from 0.45 μm filtered aqueous extracts
216 of the size-resolved aerosol samples (50% of the Berner foil in 2 ml ultrapure water), fog water, diluted
217 (1:15 000) seawater and melt pond samples using ion chromatography (ICS3000, Dionex) as described
218 by Müller et al. (2010). In this study, we discuss the results for Na^+ as a proxy for primary sea spray
219 emissions in remote marine regions. Additionally, the pH was monitored by an additional autosampler
220 sample conductivity and pH accessory (Dionex) in all seawater, melt pond and, whenever enough
221 sample volume was available, in fog water.

222 **2.6 Absorption by phytoplankton, non-algal particles and colored dissolved 223 organic matter in seawater and melt pond samples**

224 For the investigation of bio-optical parameters in seawater and melt pond samples, the particulate
225 fraction was collected by filtering the water samples (5–500 ml) onto glass-fiber filters (GF/F,
226 Whatman), while the dissolved fraction was filtered through 0.2 μm Spartan syringe filters (Whatman,
227 Germany) immediately after sampling. The GF/F filters were analyzed to determine the absorption
228 spectra (i.e. 320–844 nm, 2 nm resolution) using the quantitative filtration technique with an
229 integrative-cavity absorption meter setup (QFT-ICAM) as developed by Röttgers et al. (2016). We



230 followed the protocol by Liu et al. (2018) for the instrument used here and the determination of the
231 absorption coefficients by total particles (a_{p440}), phytoplankton (a_{ph440}) and non-algal particles
232 (a_{NAP440}) at $\lambda=440$ nm.

233 The absorption for the dissolved fraction ($a_{CDOM}(\lambda)$) between 270 and 750 nm (1 nm resolution) were
234 measured as triplicates using a long path length liquid waveguide capillary cell (LWCC) system following
235 the procedure by Lefering et al. (2017) and including the correction for salinity effects by Röttgers et
236 al. (2014) as described for our instrumentation in Álvarez et al. (2022). The absorption coefficients in
237 the visible at 443 nm ($a_{CDOM443}$) and UV at 350 nm ($a_{CDOM350}$) bands were used as indicators of CDOM
238 magnitude.

239 **2.7 Supporting observations**

240 The German research vessel *Polarstern* performs continuous meteorological surface measurements
241 during times of ship operation. For this study, we used the data from the HMP155
242 thermometer/hygrometer probe (Vaisala), the ultrasonic anemometer (Thies Clima) and the FS11
243 visibility sensor (Vaisala) each installed at a height of 29 m, 39 m and 20 m above sea level,
244 respectively. The quality-controlled data made available by the operators on the public repository
245 PANGAEA (Schmithüsen, 2018, 2019) supported the interpretation of the results of this study.

246 The 120 h back-trajectories were computed for the sampling periods of the size-resolved aerosol
247 particles and fog water events using the NOAA HYSPLIT model (Stein et al., 2015). The trajectories were
248 calculated on an hourly basis using the GDAS1 meteorological fields (Global Data Assimilation System;
249 1° latitude/longitude; 3-hourly) and at arrival heights of 50, 250 and 1000 m. Sea ice concentration
250 data were retrieved from ERDDAP (Environmental Research Division's Data Access Program), a data
251 server maintained by NOAA (National Oceanic and Atmospheric Administration). The MIZ was defined
252 here as the oceanic region with a sea ice concentration between 15 and 80%. Data on melt pond
253 fractions were accessed from the sea ice remote sensing data archive of the University of Bremen
254 (<https://data.seaice.uni-bremen.de>, Istomina (2020)).

255 **2.8 Statistics, calculations and visualization**

256 Statistical analyses, calculations and visualization were performed in OriginPro, Microsoft Excel and R
257 version 4.2.1 using the following packages: oce, ocedata, ncd4, openair, ggplot2, reshape2, scales,
258 lubridate, cmocean, maps, mapdata, rgdal, raster, RColorBrewer, sp. Time-resolved back-trajectories
259 and sea ice maps were combined using R to compute and visualize the air mass history regarding the
260 sea-ice related sea surface compartments that has been passed. Box-whisker plots represent the
261 interquartile range (box), median (horizontal line within the box), average (open square) and the
262 minimum and maximum values of the datasets (whiskers). Measured mean values are given together



263 with the calculated standard deviations (\pm). Correlations between two measured variables were
264 expressed via the Pearson correlation coefficient R . The thresholds of significance were set for the p-
265 values 0.1, 0.05, 0.01 and 0.001.

266 Enrichment factors for CCHO in the SML (EF_{SML}) relative to the corresponding bulk sample in different
267 sea-ice related sea surface compartments (ice-free, leads/polynyas, MIZ, melt ponds) were calculated
268 based on **Formula 1** with $[x]_{SML}$ and $[x]_{bulk}$ representing the concentrations of either $pCCHO$ or $dCCHO$.
269 For the calculation of enrichment factors of CCHO in aerosol particles on Berner stage y ($EF_{aer,stage y}$;
270 **Formula 2**) and fog water (EF_{fog} ; **Formula 3**) relative to the bulk water samples, the ocean was assumed
271 as the most likely source of atmospheric Na^+ . For the calculations of EF_{aer} and EF_{fog} , $CCHO_{bulk}$ and Na^+_{bulk}
272 concentrations of all individual bulk samples attributed to a certain sea-ice related sea surface
273 compartment (ice-free, leads/polynyas, MIZ, melt ponds) were averaged over the whole campaign.
274

275
$$EF_{SML} = \frac{[x]_{SML}}{[x]_{bulk}} \quad (1)$$

276
$$EF_{aer,stage y} = \frac{[x]_{aer,stage y}/[Na^+]_{aer,stage y}}{[x]_{bulk}/[Na^+]_{bulk}} \quad (2)$$

277

278
$$EF_{fog} = \frac{[x]_{fog}/[Na^+]_{fog}}{[x]_{bulk}/[Na^+]_{bulk}} \quad (3)$$

279



280 3. Results and Discussion

281 The sources of primary marine aerosol particles, and hence atmospheric marine carbohydrates, in the
282 Arctic are diverse and influenced by the prevailing sea ice conditions. Here, we present the
283 concentrations and relative compositions of CCHO in the SML and bulk water from the ice-free ocean,
284 open leads and polynyas within the pack ice, melt ponds and the MIZ. After this, the different sea-ice
285 related sea surface compartments are linked with the atmospheric CCHO found in ambient size-
286 resolved aerosol particles and fog water. Eventually, the influence of the air mass history, enrichments
287 of CCHO towards Na^+ during the sea-air transfer and secondary atmospheric transformations
288 processes altering atmospheric CCHO are discussed.

289 3.1 Sea ice influences the properties of the sea surface water

290 **Variable CCHO concentrations in the Arctic surface water.** CCHO were found in the dissolved ($d\text{CCHO}$)
291 and particulate ($p\text{CCHO}$) phases of the SML and bulk water samples collected from the ocean and the
292 melt ponds during the PS106 campaign. Among all these aqueous samples regardless of the sampling
293 environment and depth (SML versus bulk), $d\text{CCHO}$ ($13\text{--}640 \mu\text{g L}^{-1}$; $\text{mean}_{d\text{CCHO}} = 82 \pm 110 \mu\text{g L}^{-1}$; $n=70$)
294 and $p\text{CCHO}$ ($4\text{--}810 \mu\text{g L}^{-1}$; $\text{mean}_{p\text{CCHO}} = 84 \pm 160 \mu\text{g L}^{-1}$; $n=70$) were very variable. The occurring minima,
295 maxima and mean values of both, $d\text{CCHO}$ and $p\text{CCHO}$, however, ranged within the same orders of
296 magnitude. CCHO as the sum of $d\text{CCHO}$ and $p\text{CCHO}$ ranged between $22\text{--}1070 \mu\text{g L}^{-1}$
297 ($\text{mean}_{\text{CCHO}} = 166 \pm 250 \mu\text{g L}^{-1}$; $n=70$).

298 Large differences in the mean values and standard deviations of CCHO were observed among the four
299 sea-ice related sea surface compartments in the Arctic (leads/polynyas within the pack ice, MIZ, ice-
300 free ocean, melt ponds) as shown in [Figure 2a+b](#). The highest mean values for $d\text{CCHO}$ and $p\text{CCHO}$ were
301 observed in the SML of the MIZ ($\text{mean}_{d\text{CCHO, SML, MIZ}} = 190 \pm 160 \mu\text{g L}^{-1}$; $\text{mean}_{p\text{CCHO, SML, MIZ}} = 370 \pm 310 \mu\text{g L}^{-1}$;
302 $n=5$) and melt ponds ($\text{mean}_{d\text{CCHO, SML, melt ponds}} = 190 \pm 240 \mu\text{g L}^{-1}$; $\text{mean}_{p\text{CCHO, SML, melt ponds}} = 200 \pm 310 \mu\text{g L}^{-1}$;
303 $n=6$), while the SML of the lead/polynya ($\text{mean}_{d\text{CCHO, SML, lead/polynya}} = 70 \pm 75 \mu\text{g L}^{-1}$;
304 $\text{mean}_{p\text{CCHO, SML, lead/polynya}} = 70 \pm 120 \mu\text{g L}^{-1}$; $n=20$) and ice-free open ocean ($\text{mean}_{d\text{CCHO, SML, ice-free}} = 73 \pm 12 \mu\text{g L}^{-1}$;
305 $\text{mean}_{p\text{CCHO, SML, ice-free}} = 36 \pm 5 \mu\text{g L}^{-1}$; $n=4$) samples tended to contain much less CCHO.
306 The lower concentrations of the Arctic ice-free open ocean and the lead/polynya samples were rather
307 similar to the ice-free part of the Southern Ocean west of the Antarctic peninsula
308 ($\text{mean}_{d\text{CCHO, SML, Southern Ocean}} = 48 \pm 63 \mu\text{g L}^{-1}$; $\text{mean}_{p\text{CCHO, SML, Southern Ocean}} = 72 \pm 53 \mu\text{g L}^{-1}$; $n=18$; Zeppenfeld et
309 al., 2021) during the austral summer, the tropical Cape Verde ($\text{mean}_{d\text{CCHO, SML, Cape Verde}} = 85 \pm 30 \mu\text{g L}^{-1}$;
310 van Pinxteren et al. (2023)) and the Peruvian upwelling region ($\text{mean}_{d\text{CCHO, SML, Peru}} \approx 92 \pm 32 \mu\text{g L}^{-1}$;
311 Zäncker et al. (2017)). Consequently, the Arctic MIZ and melt ponds, especially the aged ones with



312 advanced microbiological activities, stood out with elevated CCHO within the Arctic and also compared
 313 to tropical and other polar regions.

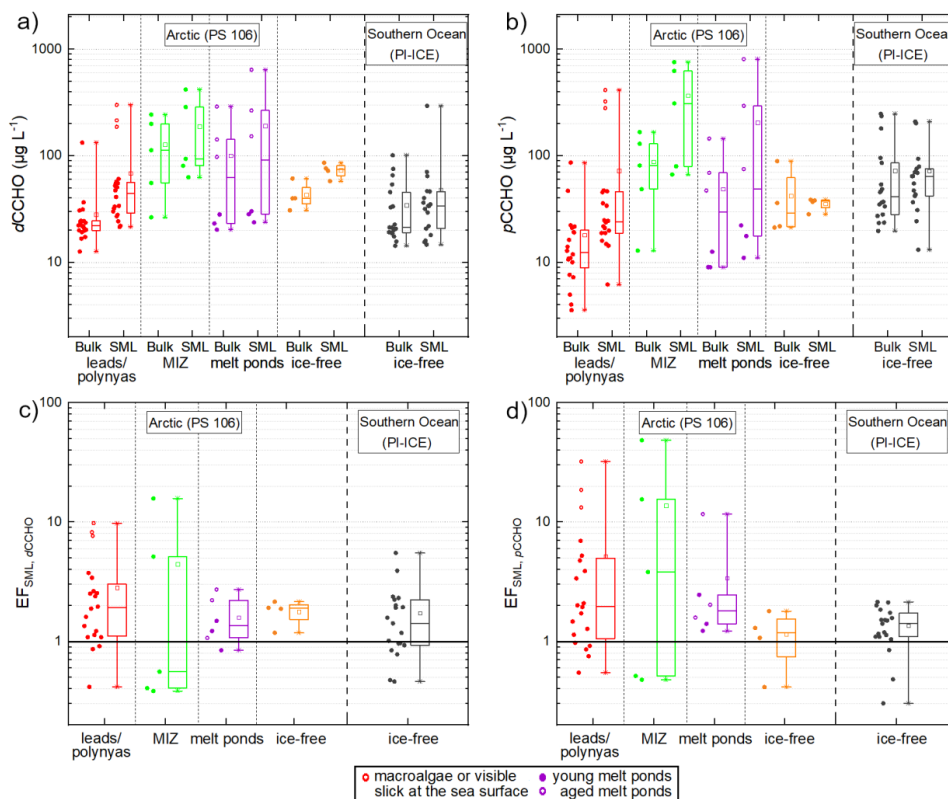


Figure 2. Scattered box-whisker plots showing the concentrations of a) $dCCHO$ and b) $pCCHO$ in the bulk and SML samples from the open leads and polynyas in the pack ice (red), the MIZ (green), ice-free open ocean (orange) and young and aged melt ponds (purple) collected during the PS106 campaign in the Arctic in comparison to the ice-free part of the Southern Ocean west of the Antarctic Peninsula investigated during the PI-ICE campaign in 2019 (black) as published in Zeppenfeld et al. (2021). EFs between SML and bulk water are shown in c) for $dCCHO$ and d) for $pCCHO$. The black horizontal line represents an $EF=1$ meaning no enrichment or depletion.

314 **Variable enrichments of CCHO in the SML.** The enrichment factors (EF_{SML}) of the CCHO in the SML
 315 relative to the corresponding bulk water ranged between 0.4 and 16 for $dCCHO$ (Figure 2c), while the
 316 EF_{SML} for $pCCHO$ varied between 0.4 and 49 (Figure 2d). The vast majority, namely 80% of the SML
 317 samples, was moderately until highly enriched in marine carbohydrates with only a few exceptions
 318 where they were depleted (7 for $dCCHO$ and 8 for $pCCHO$ out of 35 in total). With a median
 319 $EF_{SML,pCCHO,MIZ}$ of 3.8 and a mean of 13.8, the enrichment of $pCCHO$ in the MIZ stood out in contrast to
 320 the $pCCHO$ of other sea-ice related sea surface compartments and $dCCHO$ in general. However, it
 321 should be noted that the number of MIZ samples was low and median and mean values were
 322 dominated by three sample pairs with very high EF_{SML} values. Low to moderate enrichments for $dCCHO$
 323 and $pCCHO$ were typically found in the lead/polynya samples from the pack ice (median



324 $EF_{SML,dCCHO,leads/polynyas}=1.9$; median $EF_{SML,pCCHO,leads/polynyas}=2.0$, $n=20$). However, three lead samples
325 showed quite high $dCCHO$ & $pCCHO$ concentrations in the SML compared to the corresponding bulk
326 samples resulting in high $EF_{SML,dCCHO,leads/polynyas}$ up to 10 and $EF_{SML,pCCHO,leads/polynyas}$ up to 32. The
327 exceptionally high EFs of these three samples can be explained by the observation of slicks - visible
328 films on the sea surface with altered reflectance and typically high enrichments of organics (Cunliffe
329 et al., 2013; Stolle et al., 2010; Williams et al., 1986; Wurl et al., 2009) as well as the presence of
330 macroalgae floating at the ocean's surface near the sampling site. Even though the macroalgae were
331 not collected themselves, their exudates or fragments might have been released, accumulated and
332 distributed in the SML close-by and thus sampled. Consequently, the few samples with high EFs in open
333 leads might rather represent exceptional events as spatially small-scale phenomena.

334 The slight to high enrichments for $dCCHO$ and $pCCHO$ in this study are in good agreement with the
335 values reported by Gao et al. (2012), who determined $EF_{SML,dCCHO}$ between 3.5 and 12, and $EF_{SML,pCCHO}$
336 between 1.7 and 7.0 for open leads within the central Arctic Ocean. Furthermore, the $EF_{SML,dCCHO}$ of the
337 four Arctic sea ice-related sea surface compartments reported here were not significantly different
338 compared to values found in the ice-free part of the Southern Ocean (ANOVA, one-way, 0.05
339 significance level). For the $pCCHO$, however, the average EF_{SML} in the Arctic MIZ was significantly higher
340 than the one of the Southern Ocean, whereas the $EF_{SML,pCCHO}$ of the ice-free ocean in the Arctic were
341 similar to the Southern Ocean.

342 For explaining the accumulation in the SML, previous studies proposed several mechanisms and
343 processes, which fundamentally differ for the dissolved and particulate carbohydrates. The enrichment
344 of $pCCHO$ in the SML might be dominated by an interplay of density-related and wind-driven processes.
345 For instance, the positive buoyancy of TEP, a subgroup of $pCCHO$, leads to an upward flux serving as a
346 continual vehicle for marine organisms and attached chemical compounds (Azetsu-Scott and Passow,
347 2004; Mari et al., 2017). Furthermore, strong winds can cause a short-term mixing of the upper water
348 column reducing the EF_{SML} of particulates (Obernosterer et al., 2008) or TEP (Wurl et al., 2009; Zäncker
349 et al., 2021), while the wind-induced entrainment of air and the bubbling of seawater convert dissolved
350 negatively charged $dCCHO$ and colloids into larger aggregates due to their sticky properties leading to
351 an enrichment of $pCCHO$ in the SML (Passow, 2002; Robinson et al., 2019; Wurl et al., 2011). The
352 enrichment of $dCCHO$ and also $dFCHO$ in the SML is attributed to co-adsorption to other surface-active
353 compounds from the seawater matrix being scavenged at the surface of rising bubbles (Burrows et al.,
354 2016; Hasenecz et al., 2020; Schill et al., 2018; Xu et al., 2023). Additionally, microbial processes in the
355 SML could enhance the enrichment by in-situ formation and release of $dCCHO$ by micro- or
356 macroalgae, while photolysis and enzymatic degradation of $dCCHO$ to $dFCHO$ by heterotrophic
357 bacteria would lead to a reduction of the enrichment in the SML. Specific to the Arctic, the release of



358 meltwater from the sea ice could be an additional source for carbohydrates in the SML, considering
359 the production of CCHO, exopolymeric substances (EPS) and TEP by sea ice algae and bacteria as a
360 protection strategy against freezing damage and fluctuating salinity in sea ice (Aslam et al., 2016;
361 Galgani et al., 2016; Krembs et al., 2002; Krembs and Deming, 2008). This could explain the
362 extraordinarily high EF_{SML} observed in some, but not all, samples from the MIZ and melt ponds. In
363 summary, several processes might be responsible for enrichment processes in the SML, especially in
364 the Arctic, where the melting of sea ice could strongly bias the physiochemical processes usually
365 observed in controlled tank experiments.

366 **High and low salinities due to freezing and melting of sea ice.** While the surface seawater of the Arctic
367 Ocean is very saline, the Arctic sea ice is much fresher due the separation into salt-free ice crystals and
368 a salty brine during its formation from seawater and a subsequent salt loss from gravity drainage in
369 winter and flushing during summer (Notz and Worster, 2009). During the late spring and summer
370 period of this study, when strong melting of sea ice occurs, a large amount of freshwater enters the
371 surface of the ocean creating inhomogeneities of salinity within the surface of the ocean. In both the
372 ice-free ocean and the pack ice, where sea ice exists, but the melting rate is low, salinities of the SML
373 and the bulk water ranged in this study between 30.9 and 34.5 (Zeppenfeld et al., 2019b), which is
374 typical for the SML and the surface bulk water of the Arctic Ocean (Vaqué et al., 2021). Within the MIZ,
375 where freshwater from melting sea ice quickly mixes with the salty ocean water, salinities were similar
376 with values in this study between 30.1 and 33.4, however, also with an exception in the SML of 25.7.
377 Melt ponds that were not yet joined at the bottom with the ocean below, were much fresher with
378 lower and more variable salinities ranging from 4.3 to 19.5 (Zeppenfeld et al., 2019b). With a few
379 exceptions, salinity discrepancies between the SML and the corresponding bulk water were small in
380 most cases.

381 Sea-air transfer studies usually refer to open ocean scenarios with high salinities in the seawater and
382 without the presence of melting sea ice. For the calculation of enrichment factors of organics in aerosol
383 particles (EF_{aer}) or fog (EF_{fog}), the concentrations of Na^+ – a major compound of sea salt – in the
384 seawater bulk is included by default (see equations 2 and 3). However, the Arctic is a more complex
385 marine environment where salinities, and hence Na^+ concentrations, can vary widely as melting
386 progresses. This may strongly influence the mechanisms behind the bubble bursting process, the
387 CCHO/ Na^+ ratios in the bulk seawater and the SML, and thus also the EF_{aer} and EF_{fog} as it will be
388 discussed in section 3.4. Consequently, the variability of salinity in Arctic seawater and melt ponds
389 should be considered for sea-air transfer studies that rely on Na^+ values.

390 **Four sea-ice related sea surface compartments with different characteristics.** In a nutshell, the high
391 Arctic differs from other oceanic regions in the presence, formation and melting of sea ice creating



392 sea-ice related sea surface compartments (ice-free, leads/polynyas, MIZ, melt ponds) with individual
393 biological and chemical characteristics, such as CCHO concentrations, enrichments in the SML and
394 salinities. This might potentially impact the transfer of substances from the ocean to the atmosphere,
395 chemo-selective enrichment processes of marine CCHO in the primary marine aerosol particles and
396 thus their microphysical properties. The next chapters will elucidate if and how these differences
397 within the individual compartments relate to $CCHO_{aer}$ and $CCHO_{fog}$.



398 **3.2 Sea spray aerosol and therein contained combined carbohydrates**

399 ***Breaking waves as the main mechanism for SSA emissions is not unambiguous in the Arctic.*** In the
400 open ocean, the emission flux of SSA and hence its inorganic and organic constituents mainly depends
401 on the wind speed as the driving force for breaking waves and bubble bursting, and furthermore on
402 the seawater temperature, salinity, wave properties and organic surface-active substances (Grythe et
403 al., 2014). In this study, atmospheric sodium ($\text{Na}^+_{\text{aer,PM}_{10}}$), the best tracer for SSA (Barthel et al., 2019),
404 ranged between 12 and 765 ng m^{-3} (Table SI 1). $\text{Na}^+_{\text{aer,PM}_{10}}$ showed a good correlation ($R=0.80$, $p<0.001$,
405 Figure SI 2a) with wind speed, measured at the sampling site and averaged over the sampling time, if
406 all aerosol samples are included. However, the strength of this correlation decreased sharply ($R=0.59$,
407 $p<0.1$), when only samples collected over the MIZ and the pack ice were included, while the few
408 samples from the open ocean characterized by high Na^+ values were excluded. This is due to the
409 presence of sea ice in the high Arctic, which likely alters and conceals the classical wind-driven
410 mechanisms of breaking waves and bubble bursting resulting in SSA emission. Firstly, sea ice covers a
411 significant part of the Arctic Ocean strongly reducing the area releasing SSA. Secondly, the presence of
412 sea ice causes an attenuation of the high-frequency wind-sea waves, while longer waves, such as
413 swells, can remain (Thomson, 2022). Consequently, the effect of wind on the SSA emission mechanisms
414 within the open leads and the MIZ might be different than in the ice-free ocean. For those sea-ice
415 dominated compartments, alternative wind-independent sources of ascending bubbles were
416 suggested, such as melting sea ice nearby, respiration of phytoplankton or sea-air heat exchange below
417 the sea surface (Chen et al., 2022 and references therein). Thirdly, in contrast to other marine regions
418 with quite homogeneous ocean salinities, and hence sodium concentrations, the salinities among the
419 different Arctic sea-ice related sea surface compartments are more variable due to the melting of sea
420 ice. Previously, the results of a sea-air transfer tank experiment with artificial seawater showed the
421 influence of salinity on the relative particle number concentrations of emitted SSA for salinities below
422 15 – values especially relevant for melt ponds in the Arctic – while changes at higher salinities did not
423 result in a measurable effect (Zábori et al., 2012). Additionally, organics with potential surface-active
424 properties are very variable in these disparate Arctic environments, as discussed for CCHO in chapter
425 3.1. Organic surfactants can alter the ocean surface's ability to form whitecaps and the lifetime of
426 bubbles (Bigg and Leck, 2008; Callaghan et al., 2012; Grythe et al., 2014) and therefore SSA properties.

427 Finally, blowing snow over the sea ice could serve as an additional, non-oceanic source of atmospheric
428 Na^+_{aer} when a certain air-temperature-dependent wind speed threshold is exceeded (Chen et al., 2022;
429 Yang et al., 2008). Consequently, connections and correlations for the release of SSA particles in the
430 heterogeneous high Arctic are more difficult to explore than other marine environments without sea



431 ice. It can be assumed that this complex setting does not only influence the release of the inorganic
432 constituents from seawater, but its organic compounds, such as CCHO, too.

433 **CCHO_{aer} distributed in all size modes.** During the PS106 campaign, the overall atmospheric
434 concentrations of CCHO_{aer,PM10} ranged between 0.5 and 4.7 ng m⁻³ (Table SI 1). Combined
435 carbohydrates were found on both supermicron (CCHO_{aer,super}=0.07–2.1 ng m⁻³) and submicron
436 particles (CCHO_{aer,sub}=0.26–4.4 ng m⁻³). Thus, these CCHO_{aer} values ranged within the same orders of
437 magnitude as in the Arctic studies by Karl et al. (2019) and Leck et al. (2013) or the study conducted at
438 the western Antarctic peninsula by Zeppenfeld et al. (2021a). CCHO_{aer} appeared in all of the five size
439 classes in variable concentrations (Figure 3a). Although the average concentrations were similar on all
440 stages, local maxima were observed on stages 2 (0.14–0.42 μm) and 5 (1.2–10 μm). A similar size
441 distribution of marine CCHO_{aer} in these specific size ranges, but more pronounced, has been already
442 observed in the ice-free part of the Southern Ocean by Zeppenfeld et al. (2021a) explaining these
443 findings with a likely release of marine polysaccharides from the ocean as part of film and jet droplets.
444 Possibly, the aerosol size distribution of marine polysaccharides resulting from wind-driven bubble
445 bursting emissions are not as obvious in this Arctic study as it was in the ice-free Southern Ocean due
446 to the presence of Arctic sea ice suppressing and altering the local SSA emission mechanisms as
447 indicated in the previous section. The relative contribution of CCHO_{aer} to mass_{aer} varied between 0.01%
448 and 4% (Figure 3b), while the carbon contained within the combined carbohydrates (C-CCHO_{aer})
449 contributed 0.06 to 4.9% to the OC_{aer} in the size-resolved aerosol particles (Figure 3c). These
450 contributions agree well with the findings in marine aerosol particles from the Southern Ocean
451 (Zeppenfeld et al., 2021a).

452

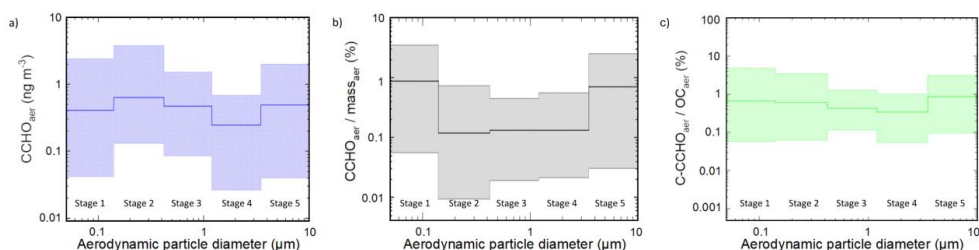
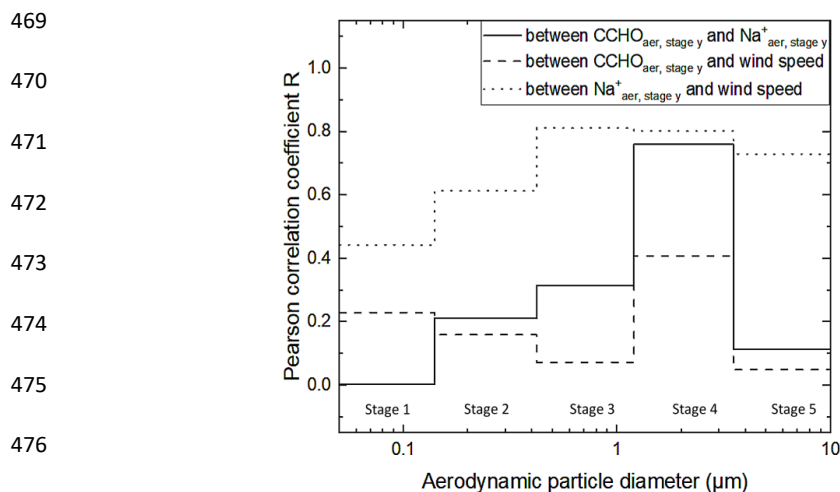


Figure 3. a) Concentration of combined carbohydrates in size-resolved aerosol particles (CCHO_{aer}), b) ratio of CCHO_{aer} to the total particle mass concentration (mass_{aer}), c) ratios of carbon contained within the combined carbohydrates in aerosol particles (C-CCHO_{aer}) to organic carbon in aerosol particles (OC_{aer}). The bold lines represent the average concentrations during the PS106 campaign. The hatched areas show the range between the maximum and minimum values. The aerodynamic particle diameter refers to sampling conditions at relative humidity of max. 80%.

453 Unlike the study conducted in the Southern Ocean (Zeppenfeld et al., 2021a), CCHO_{aer,PM10} in this study
454 showed no significant correlations with Na⁺_{aer,PM10} (R=0.24, p>0.1, Figure SI 2b) or wind speed (R=0.26,
455 p>0.1, Figure SI 2c), which could be due to the complex marine environment and the relevance of



456 several emission mechanisms in the Arctic as discussed above. However, if the correlations are
 457 resolved for the different Berner impactor stages (i.e. size ranges), a large variability can be observed
 458 (Figure 4). A higher correlation was found especially on stage 4 (1.2–3.5 μm) between $\text{CCHO}_{\text{aer,stage } 4}$
 459 and $\text{Na}^+_{\text{aer,stage } 4}$ ($R=0.76$, $p<0.01$), while the Pearson correlations coefficients for the other Berner
 460 stages were much lower. This could indicate the same marine source and wind-driven emission
 461 mechanism for both chemical constituents in this supermicron aerosol size mode, while other aerosol
 462 size modes might have been influenced by atmospheric aging and wind-independent emission
 463 mechanisms as already mentioned for Na^+_{aer} in the previous section. This observation agrees well with
 464 the findings by Bigg and Leck (2008) and Leck (2002) reporting submicron polymer gel particles, likely
 465 consisting of polysaccharides, in the atmosphere of the high Arctic containing almost no sea salt and
 466 showing large similarities to those particles found in open leads close-by. This is quite surprising
 467 considering that the mechanism of wind-driven wave breaking is quite limited due to the lack of long
 468 fetches of open water (Held et al., 2011; Norris et al., 2011).



476 **Figure 4.** Pearson correlation coefficient R between $\text{CCHO}_{\text{aer,stage } y}$ and $\text{Na}^+_{\text{aer,stage } y}$ (solid line), between $\text{CCHO}_{\text{aer,stage } y}$ and the average wind speed (dashed line), and between $\text{Na}^+_{\text{aer,stage } y}$ and the average wind speed (dotted line) for each stage y of the Berner impactor.

477 Blowing snow has been discussed as a possible additional source for atmospheric Na^+ , raising the
 478 question, if it could be a source for atmospheric carbohydrates, too. During this study, the
 479 measurements of $d\text{FCHO}$ and CCHO in five Arctic snow samples collected resulting in low values mostly
 480 below the limits of detection. This finding supports the conclusion that blowing snow does not serve
 481 as a competitive source for the emission of atmospheric carbohydrates.



482 3.3 Marine combined carbohydrates in fog

483 The concentrations of $\text{Na}^+_{\text{fog, liquid}}$ ($1.7\text{--}903 \text{ mg L}^{-1}$; mean = $130\pm 220 \text{ mg L}^{-1}$; $n=22$) and $\text{CCHO}_{\text{fog, liquid}}$
484 ($18\text{--}22000 \text{ } \mu\text{g L}^{-1}$; mean = $1380\pm 4600 \text{ } \mu\text{g L}^{-1}$; $n=22$) were very variable in fog water (Table SI 2).
485 Atmospheric fog concentrations of these chemical constituents can be calculated under consideration
486 of the liquid water content (LWC) during the fog events. Since LWC was not measured during PS106
487 directly, the LWC was approximated from the measured CCN concentrations at the lowest quality
488 assured supersaturation of 0.15% and an assumed average droplet diameter of $17 \text{ } \mu\text{m}$ resulting in a
489 LWC of $0.20\pm 0.27 \text{ g m}^{-3}$ (Hartmann et al., 2021). Following this approach, atmospheric concentrations
490 in fog ranged between 0.12 and $150 \text{ } \mu\text{g m}^{-3}$ (mean = $25\pm 43 \text{ } \mu\text{g m}^{-3}$; $n=16$) for $\text{Na}^+_{\text{fog, atmos}}$ and between
491 3 and 4300 ng m^{-3} (mean = $390\pm 1100 \text{ ng m}^{-3}$; $n=16$) for $\text{CCHO}_{\text{fog, atmos}}$, respectively. These atmospheric
492 concentrations in fog are for both $\text{Na}^+_{\text{fog, atmos}}$ and $\text{CCHO}_{\text{fog, atmos}}$ by one to three orders of magnitude
493 higher than the atmospheric concentrations in aerosols discussed in section 3.2. This divergence may
494 be explained by the following:

- 495 - Fog scavenging is a transfer process of aerosol particles into the liquid phase of fog droplets
496 (Gilardoni et al., 2014). As fog forms and grows, it can capture aerosol particles in the air and
497 increase their concentration within the fog droplets. This could lead to higher atmospheric
498 concentrations of aerosol particle compounds, especially for the water-soluble and
499 hygroscopic ones, inside the fog compared to the surrounding air.
- 500 - The activation of aerosol particles to fog droplets is a process dominated by particle size with
501 larger particles tending to activate first. It is conceivable that SSA particles larger than $10 \text{ } \mu\text{m}$,
502 usually few in number, but with a large mass contribution, were available near the sea surface,
503 where sampling occurred. These SSA particles were activated into fog droplets and contributed
504 significantly to the Na^+ and CCHO in the fog. In contrast, aerosol sampling was restricted by
505 the Berner impactor's $10 \text{ } \mu\text{m}$ diameter cut-off neglecting the larger particles in the
506 consideration.
- 507 - The LWC values were not measured but estimated, which could be a source of errors.
508 However, the calculated LWC values ranged within a realistic frame for Arctic fog and likely are
509 not responsible for the large difference between aerosol and fog concentrations in several
510 orders of magnitude.

511 Since both, organic and inorganic constituents, showed higher atmospheric concentrations in
512 fog/clouds compared to ambient aerosol particles, we conclude that a physical phenomenon, such as
513 fog scavenging, might explain this observation and not an in-situ formation within the cloud droplets.
514 Similar to the findings of this study discussing marine CCHO and Na^+ in Arctic fog, Triesch et al. (2021a)



515 found strikingly high concentrations of free amino acids (FAA) and Na⁺ in marine clouds compared to
516 aerosol particles both collected on top of the Mt. Verde on Cape Verde Islands as shown in [Table 1](#).

517 While *d*FCHO_{fog} and derivatives, such as anhydrosugars and sugar alcohols, have been readily reported
518 for fog water with terrestrial and marine background (Dominutti et al., 2022), we here present for the
519 first time ambient CCHO concentrations in marine fog.

520 **Table 1.** Atmospheric concentrations of selected SSA constituents in fog/clouds compared to ambient aerosol particles during
521 marine field studies.

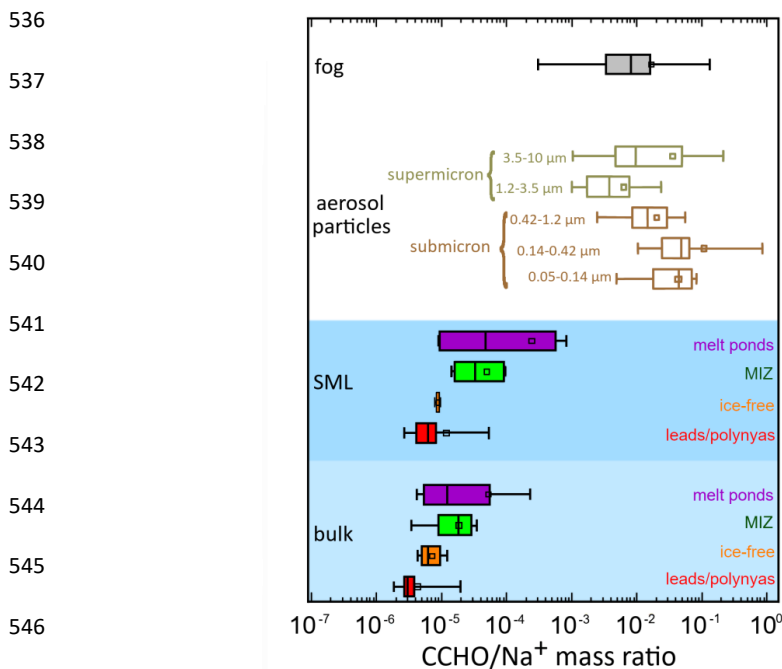
Chemical constituent	Fog/cloud (ng m ⁻³)	PM ₁₀ (ng m ⁻³)	Sampling location	Sampling height	Sampling period	Reference
<i>d</i> FCHO	9.2–52 ^{a,b}	–	Reúnion	1760 m a.s.l. ^d	March–April 2019	Dominutti et al. (2022)
	1.5–1040 (mean:80±260)	<LOD–2.0	Arctic	25 m a.s.l. ^e	May–July 2017	this study
CCHO	3–4300 (mean:390±1100)	0.5–4.7	Arctic	25 m a.s.l. ^e	May–July 2017	this study
FAA	11–490	1.0–4.8	Cape Verde	744 m a.s.l. ^f	Sept.–Oct. 2017	Triesch et al. (2021a)
	6–79	–	Reúnion	1760 m a.s.l. ^d	March–April 2019	Dominutti et al. (2022)
	(µg m ⁻³)	(µg m ⁻³)				
Na ⁺	1.6–7.2	0.17–0.40	Cape Verde	744 m a.s.l. ^f	Sept.–Oct. 2017	Triesch et al. (2021a)
	0.1–2.2 ^b	–	Reúnion	1760 m a.s.l. ^d	March–April 2019	Dominutti et al. (2022)
	0.014–0.063 ^c	–	Arctic	180–374 m ^g	Aug.–Sept. 2018	Zinke et al. (2021)
	0.12–150 (mean:25±43)	0.012–0.77	Arctic	25 m a.s.l. ^e	May–July 2017	this study

522 ^aonly includes free glucose and rhamnose; sugar alcohols and anhydrosugars were not included for this table. ^bvalues were
523 calculated from LWCs, molecular weights and concentrations in fog water given within the reference; terrestrial contributions
524 are likely. ^ccalculated from concentration in fog water and an assumed LWC of 0.1 g m⁻³. ^dPiste Omega. ^eRV *Polarstern*. ^fMt.
525 Verde. ^gtethered balloon.



526 **3.4 Chemo-selective sea-air transfer of marine carbohydrates**

527 The chemo-selective sea-air transfer of organics towards inorganic sea salt constituents has been
 528 described both in tank and ambient field studies for organic carbon in general (Gantt et al., 2011;
 529 Hoffman and Duce, 1976; van Pinxteren et al., 2017) or several chemical constituents, such as
 530 carbohydrates (Hasenecz et al., 2020; Schill et al., 2018; Zeppenfeld et al., 2021a), lipids (Triesch et al.,
 531 2021b) and free and combined amino acids (Triesch et al., 2021a, c). The calculation of dimensionless
 532 ratios between the concentrations of the examined organic parameter and Na^+ allows a comparison
 533 of aquatic and atmospheric samples within the marine environment. **Figure 5** shows the CCHO/Na^+
 534 ratios for the bulk and SML in the four sea-ice related sea surface compartments, size resolved aerosol
 535 particles and fog water collected during the PS106 cruise.



546 **Figure 5.** CCHO/Na^+ ratios for CCHO in Arctic fog, size-resolved aerosol particles and the surface seawater (SML and bulk) from melt ponds, the marginal ice zone (MIZ), the ice-free ocean and leads/polynyas from the pack ice.

547 **Wide range of CCHO/Na^+ ratios in Arctic surface seawater.** In the surface seawater samples of this
 548 study, the CCHO/Na^+ ratios spanned from 2×10^{-6} to 8×10^{-4} , representing a wider range than those
 549 found in the Southern Ocean (9×10^{-7} and 3×10^{-5} ; Zeppenfeld et al., 2021). While the ratios in the SML
 550 and bulk water in general ranged in the same orders of magnitude, large differences were observed in
 551 the individual Arctic sea-ice related sea surface compartments. In the SML, lowest median values were
 552 found in the leads/polynyas and ice-free ocean samples with 6×10^{-6} and 9×10^{-6} , respectively, while
 553 higher median values appeared in the SML of the MIZ (3×10^{-5}) and melt ponds (4×10^{-5}), or even



554 6×10^{-4} , when only aged melt ponds were considered. This large variability of CCHO/Na⁺ ratios can be
555 explained by the variable content of CCHO (high CCHO content in aged melt ponds & MIZ versus ice-
556 free ocean & leads/polynyas) and Na⁺ (low salinity in the SML of melt ponds versus higher salinities in
557 ice-free ocean & leads/polynyas & MIZ) in the different sea-ice related sea surface compartments. It
558 can be expected, that the different CCHO/Na⁺ ratios in the individual seawater compartments
559 impacted the corresponding CCHO/Na⁺ ratios in fog and aerosol particles during the sea-air transfer,
560 and consequently the enrichment factors for the sea-air transfer (EF_{aer} , EF_{fog}), which are calculated
561 from those ratios.

562 ***Air mass history influences CCHO_{aer}/Na⁺_{aer} ratios in Arctic aerosol particles.*** In contrast to the
563 seawater samples, CCHO_{aer}/Na⁺_{aer} ratios were much higher for aerosol particles considering the size
564 resolution (1×10^{-3} – 9×10^{-1}) supporting the concept of the chemo-selective enrichment of
565 carbohydrates towards Na⁺ during the transfer from the ocean into the atmosphere. In this context,
566 submicron particles showed much higher median ratios of 4×10^{-2} (0.05–0.14 μm) and 4×10^{-2}
567 (0.14–0.42 μm) than supermicron particles with 4×10^{-3} (1.2–3.5 μm) and 1×10^{-2} (3.5–10 μm).
568 Considering PM₁₀ (sum of all five Berner stages), the CCHO_{aer,PM10}/Na⁺_{aer,PM10} ratios varied much more
569 in the Arctic study presented here (2×10^{-3} – 2×10^{-1} , see [Table SI 1](#)) than in the ice-free part of the
570 Southern Ocean (8×10^{-4} – 7×10^{-3} ; Zeppenfeld et al. (2021b)). Interestingly, in the four aerosol sampling
571 periods (24/05/17–26/05/17; 26/05/17–29/05/17; 29/05/17–01/06/17; 19/06/17–25/06/17) where
572 the air masses had passed the majority (45–100%) of the previous 12 h before sampling over the open,
573 ice-free ocean (trajectories combined with sea ice maps can be found in [Figure SI 3](#)) exhibited the
574 lowest CCHO_{aer,PM10}/Na⁺_{aer,PM10} ratios (2×10^{-3} – 9×10^{-3} , see [Table SI 1](#)), very similar to the values in the
575 ice-free Southern Ocean. In contrast, higher ratios were found, when the air masses had rested a
576 significant time over the pack ice or the MIZ. This could be an indication that the chemical composition
577 of the sea-ice related sea surface compartments, here the ice-free ocean with low CCHO/Na⁺ ratios,
578 strongly influences the relative composition of aerosol particles. In contrast, the influence of the MIZ,
579 pack ice and melt ponds exhibiting quite different chemical, physical and biological properties on
580 CCHO_{aer,PM10}/Na⁺_{aer,PM10} could not be resolved in further details following this approach using trajectory
581 calculation and satellite data. This is certainly due to the proximity of these sea-ice related sea surface
582 compartments on a small spatial scale (especially melt ponds in direct vicinity to open leads), the long
583 sampling periods of aerosol particles, the lacking knowledge of deposition rates, the effect of wind on
584 bubble bursting processes within the individual sea-ice related sea surface compartments and missing
585 data on the biological activities in individual melt ponds.

586 ***Similar CCHO/Na⁺ ratios in aerosol particles and fog.*** For fog, CCHO_{fog}/Na⁺_{fog} ratios ranged from
587 3×10^{-4} to 1×10^{-1} , which covers the same orders of magnitude of aerosol particles. Even though absolute



588 atmospheric concentrations of CCHO are much higher in fog than in aerosol particles possibly due to
589 fog scavenging (as discussed in 3.3), the CCHO/Na⁺ ratios are similar. This strongly implies that CCHO_{fog}
590 actually originated from the ambient marine aerosol particles. The attempt to find matches or common
591 trends between aerosol particles and the fog in individual samples was not successful, certainly due to
592 the very different resolutions of sampling times and in addition due to the probability of fog droplets
593 containing aerosol particles bigger than 10 μm.

594 **Calculated EF_{aer} and EF_{fog} depend on the sea-ice related marine source under consideration.** EF_{aer} and
595 EF_{fog} are calculated as a quotient between the CCHO/Na⁺ ratios in the size-resolved aerosol
596 particles/fog and the corresponding bulk water. The concentrations in the Arctic seawater of this study
597 was very variable depending on the regarded sea-ice related sea surface compartment environment,
598 as well in the aerosol particles and in fog water. This fact strongly impacted the resulting EF_{aer} and EF_{fog} ,
599 enabling calculated values ranging between 10¹ and 10⁴ for supermicron aerosol particles, between
600 10² and 10⁵ for submicron particles and between 10⁰ and 10⁴ for fog depending on which sea-ice
601 related sea surface compartment was assumed as the marine source of SSA as shown in [Figure 6](#).
602 Lower atmospheric EFs were calculated when aged melt ponds ($EF_{aer,super}=19-750$; $EF_{aer,sub}=127-5100$;
603 $EF_{fog}=5-2400$) or the MIZ ($EF_{aer,super}=60-2310$; $EF_{aer,sub}=390-16000$; $EF_{fog}=17-7400$) were assumed as
604 the only (theoretical) marine source of CCHO and Na⁺, while higher values were found with the ice-
605 free ocean ($EF_{aer,super}=175-6800$; $EF_{aer,sub}=1100-46000$; $EF_{fog}=50-22000$) or open leads/polynyas
606 ($EF_{aer,super}=360-14000$; $EF_{aer,sub}=2360-95000$; $EF_{fog}=103-44600$). It is important to note that EFs were
607 most consistent with results from other CCHO sea-air transfer studies in the tank (Hasenecz et al.,
608 2020) and the field (Zeppenfeld et al., 2021a), when aged melt ponds or the MIZ were considered as
609 the oceanic emission source. If leads/polynyas and the ice-free ocean are regarded as the only emission
610 source, higher EF_{aer} and EF_{fog} values resulted, and hence the assumption of a stronger mechanistic
611 enrichment. It is highly unlikely whether an air mass package had been exclusively exposed to
612 leads/polynyas during its history, and not to aged melt ponds or the MIZ. Consequently, none of the
613 Arctic sea-ice related sea surface compartments discussed above should be neglected in the discussion
614 of sea-air transfer of organic substances.

615 During the same Arctic field campaign, Hartmann et al. (2021) investigated INP in ambient aerosol
616 particles and compared it to bulk and SML in seawater from all the different sea-ice related sea surface
617 compartments using similar EF_{aer} calculations as reported here. They concluded that an enrichment of
618 3 to 5 orders of magnitude was necessary during the sea-air transfer to fully attribute atmospheric INP
619 to oceanic sources. Here, we show that such high EF_{aer} and EF_{fog} for organics, and hence marine
620 biogenic INP, can be calculated, e.g. when open leads/polynyas were referred to as the only oceanic
621 source. In summary, Arctic air masses have been impacted by different types of sea-ice related sea



622 surface compartments before sampling, whereas it is still unclear which one has the biggest effect on
 623 the chemical composition of the marine aerosol particles. This aspect should be considered when the
 624 marine SSA constituents are modelled for the Arctic from remote sensing data.

625

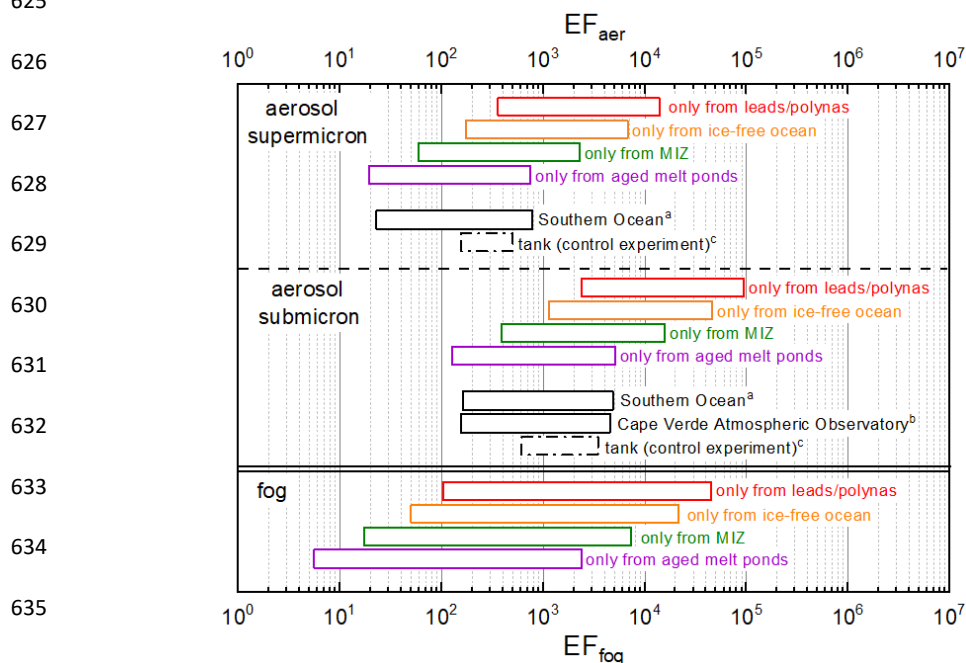


Figure 6. Range of calculated hypothetical enrichment factors EF_{aer} and EF_{fog} assuming either leads/polynyas, the ice-free ocean, the MIZ or aged melt ponds as the only marine source for the sea-air transfer of CCHO in the Arctic. For the calculation of EF_{aer} and EF_{fog} , the minimum and maximum values of the $CCHO_{aer/fog}/Na^+_{aer/fog}$ ratios and the median values of $CCHO_{bulk}/Na^+_{bulk}$ were used. The EF_{aer} values of this study were compared with the results of a) the field study conducted in the Southern Ocean by Zeppenfeld et al. (2021), b) the field study conducted at Cape Verde Atmospheric Observatory (CVAO) by van Pinxteren et al. (2023) and c) the results of the CCHO tank study by Hasenecz et al. (2020) without any addition of heterotrophic bacteria (control experiment). Here, EF_{aer} values were calculated from the experimental data published by Hasenecz et al. (2020b).

636



637 **3.5 Atmospheric aging of marine carbohydrates**

638 To resolve the fate of marine carbohydrates in the atmosphere after their ejection from the ocean, the
639 relative molar contribution of monosaccharides to CCHO were compared between the bulk and SML
640 from the leads/polynyas, MIZ, ice-free ocean and melt pond samples, as well as the sub-and
641 supermicron aerosol particles and fog water (Figure 7). The composition of marine carbohydrates in
642 seawater strongly depends on the dominating microbial species, season, diagenetic state, availability
643 of nutrients and environmental stress factors (Engbrodt, 2001; Goldberg et al., 2011) leading to a
644 natural variability among individual samples even within small spatial scales. Consequently, to enable
645 the direct comparison of seawater with atmospheric samples of this field study with an elevated level
646 of statistical certainty, here we compare the mean values of the entire data set, instead of individual
647 samples. Finally, in addition to the changes of the monosaccharide patterns of CCHO, the systematic
648 degradation of CCHO to *d*FCHO was observed in the atmosphere and will be discussed within this
649 chapter.

650 ***CCHO composition in different sea-ice related sea surface compartments and depths is similar.*** In
651 seawater (bulk and SML), glucose (means= 35–48 mol%), galactose (means= 13–18 mol%) and xylose
652 (means= 7–16 mol%) dominated the CCHO composition followed by smaller contributions of other
653 neutral sugars, amino sugars, uronic acids and muramic acid (Figure 7). Considering the natural
654 variability among individual samples, there were no significant differences in means between the bulk
655 and SML, nor between the lead/polynya, MIZ, ice-free ocean and melt pond samples. Variations were
656 observed between the dissolved and particulate fractions (Figure SI 6), nevertheless the combined
657 carbohydrates within all sea-ice related sea surface compartments followed the same pattern of the
658 predominance of glucose, galactose and xylose. Overall, the relative monosaccharide compositions of
659 glucose > (galactose ≈ xylose) > other (neutral or charged) monosaccharides of the seawater samples
660 from this Arctic study appear similar to the monosaccharide compositions investigated in the SML and
661 bulk water from the Central Arctic Ocean (Gao et al., 2012) and at the western Antarctic peninsula
662 (Zeppenfeld et al., 2021a), the meltwater of Arctic multiyear sea ice (Amon et al., 2001) and the
663 epipelagic water from the Ross Sea (Kirchman et al., 2001).

664 ***Less galactose, but more muramic acid in atmospheric CCHO_{aer} and CCHO_{fog}.*** Atmospheric samples
665 showed a different monosaccharide pattern within the hydrolyzed CCHO in comparison to the
666 seawater and melt pond samples. While glucose (means= 41; 50 and 60 mol% for fog, submicron and
667 supermicron aerosol particles, respectively) and xylose (means= 16; 15 and 15 mol%) still prevailed
668 over the relative monosaccharide pattern, the contribution of galactose (means= 6; 3 and 3 mol%) was
669 strongly reduced, both in fog and aerosol particles. On the other hand, the ratio of muramic acid was

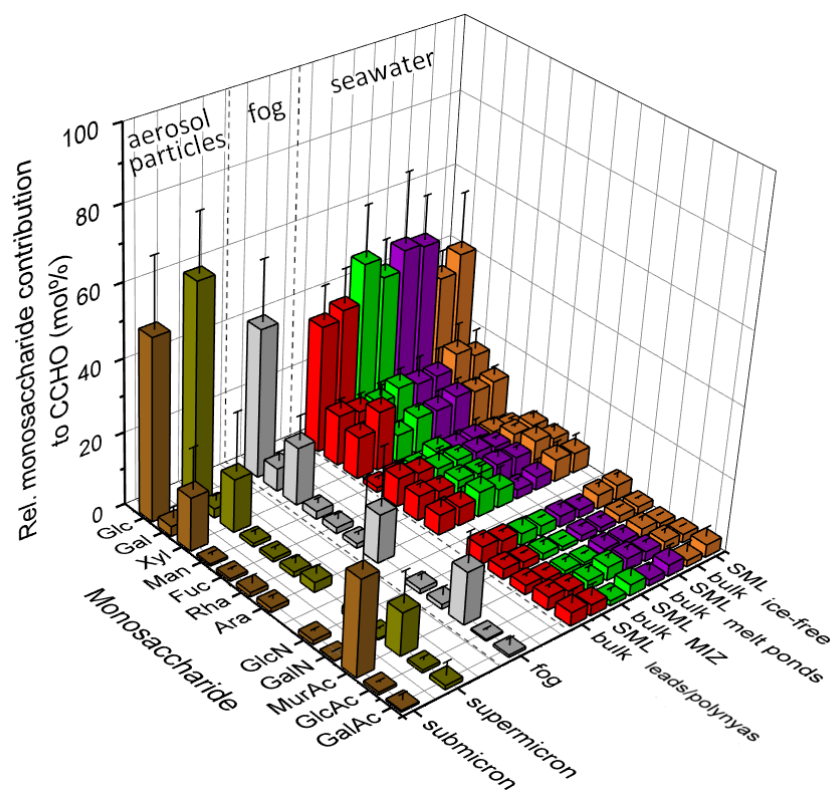


Figure 7. Relative monosaccharide composition of combined carbohydrates (CCHO) after acid hydrolysis in sub-/ supermicron aerosol particles, fog water, bulk and SML samples from the leads and polynyas within the pack ice, the MIZ, the ice-free ocean and young and aged melt ponds. The 3D bar chart shows the averages and standard deviations of the relative contributions. Glc: glucose, Gal: galactose, Xyl: xylose, Man: mannose, Fuc: fucose, Ara: arabinose, GlcN: glucosamine, GalN: galactosamine, MurAc: muramic acid, GlcAc: glucuronic acid, GalAc: galacturonic acid.

670 strongly elevated in aerosol particles (means= 12 and 26 mol%) and fog water (mean= 14 mol%) in
 671 comparison to the oceanic samples (means= 0.9–2.6 mol%). These differences of the relative
 672 monosaccharide contributions to CCHO among the seawater and the atmospheric samples described
 673 within this study are in good agreement with the sea-air transfer investigations conducted in the
 674 Southern Ocean at the western Antarctic peninsula (Zeppenfeld et al., 2021a). Consequently, the
 675 occurring phenomenon might be independent from the sampling location and could be explained by
 676 three possible atmospheric processes, such as (1) a chemo-selective sea-air transfer of certain oligo-
 677 or polysaccharides over others, (2) an atmospheric transformation due to abiotic chemical reactions
 678 or (3) an atmospheric transformation due to microbiological activities. Among these possible
 679 pathways, Zeppenfeld et al. (2021) presumed the secondary atmospheric transformation caused by
 680 microbiological metabolism as the most probable or at least most dominant one supported by the
 681 prevalence of muramic acid, an amino sugar acid naturally occurring in bacterial cell walls (Mimura



682 and Romano, 1985; Sud and Tyler, 1964), and the very selective absence of certain monosaccharides
683 in the CCHO_{aer} in aerosol particles as it was observed in this Arctic study as well.

684 **Formation of combined arabinose in fog.** A comparison of the monosaccharide composition of aerosol
685 particles and fog water showed great similarity regarding dominant contributions from glucose, xylose
686 and muramic acid. It seems plausible that the fog water droplets contained the same inorganic and
687 organic compounds found in the SSA particles assuming that SSA particles activated the formation of
688 fog droplets as CCN due to their rather large diameters and high hygroscopicity. Apart from that,
689 however, a significant difference was observed in the increased relative contribution of arabinose in
690 fog (mean= 13 mol%) compared to aerosol particles (means= 1.2 and 2.7 mol%) indicating a formation
691 of arabinose in the liquid phase. During a marine microcosm experiment performed by Hasenecz et al.
692 (2020), a strong link was observed between the release of arabinose-containing polysaccharides in
693 form of EPS and the presence of heterotrophic bacteria and stressed phytoplankton. Furthermore, a
694 strain of the psychrotolerant marine bacterium *Pseudoalteromonas* sp. has been shown to produce
695 EPS mainly composed from glucose, arabinose and xylose (Casillo et al., 2018; Qin et al., 2007).
696 Consequently, the release of arabinose-containing EPS in fog could be a plausible protection
697 mechanism of microorganisms contained within a droplet against freezing damage under low Arctic
698 temperatures.

699 **Indication for microbial activities in the atmosphere.** Intact bacterial cells at atmospheric
700 concentrations between 5×10^2 and 8×10^4 cells m^{-3} for remote marine and ice-covered regions (Šantl-
701 Temkiv et al., 2018; Mayol et al., 2017), cell-bound and free enzymes have been detected in ambient
702 and nascent marine super- and submicron aerosol particles during several field and tank studies (Aller
703 et al., 2005; Hasenecz et al., 2020; Malfatti et al., 2019; Marks et al., 2001; Rastelli et al., 2017; Šantl-
704 Temkiv et al., 2020; Uetake et al., 2020). For surviving in this hostile environment, some of these
705 microbes have developed a remarkable resilience towards extreme environmental stressors, such as
706 high UV radiation, radical exposure, changing osmolarity, freezing temperatures and desiccation. As
707 survival strategies could serve the selective enzymatic consumption of airborne labile carbohydrates
708 explaining the here observed loss of galactose and the persistence of xylose, the formation of
709 protecting biofilm from EPS, carotenoid pigmentation or the formation of own precipitating
710 hydrometeors by enabling condensation on a surface as a CCN or freezing by IN active surfaces to
711 reduce their atmospheric residence time (Delort et al., 2010; Matulová et al., 2014; Šantl-Temkiv et
712 al., 2020). Consequently, an enzymatic transformation might serve as a plausible explanation for the
713 selective removal of certain monosaccharides within CCHO_{aer} and CCHO_{fog} observed here. However,
714 the survival and the metabolic activity of microorganisms is restricted by the presence of water (Ervens
715 and Amato, 2020; Haddrell and Thomas, 2017) identifying liquid hydrometeors or fresh SSA as the



716 most biologically active atmospheric hotspots. In contrast to most of the ambient aerosol particles, fog
717 droplets provide enough water essential for bacterial activities. However, they might freeze under
718 Arctic sub-zero temperatures possibly causing damage to the microbial cells, which might explain an
719 in-situ formation of a protecting biofilm from arabinose-containing EPS. In a previous Arctic study,
720 Orellana et al. (2011) readily detected microgels in aerosol particles, cloud and fog water most likely
721 emitted from the surface water and the SML via bubble bursting. Indications for an in-situ generation
722 of marine microgels in fog water as an additional source to the primary release from the ocean by
723 bubble bursting have been observed by van Pinxteren et al. (2022) in the tropical Atlantic Ocean.

724 The selective sea-air transfer of certain carbohydrates over others and the abiotic degradation as
725 further possible pathways to the biotic transformation of marine CCHO_{air} have been discussed in detail
726 in Zeppenfeld et al. (2021), but do not appear, based on the current state of knowledge, as likely
727 explanations of the very selective CCHO degradation and formation of other CCHO observed here.
728 More future lab and mesocosm experiments are required to elucidate the contribution of each of these
729 processes. Finally, the similarity of the carbohydrate composition of fog water and aerosol particles,
730 both two atmospheric compartments collected with different instrumentation, allows to rule out
731 artefacts of the different sampling and extraction techniques as a reason for the observed differences
732 to the seawater.

733 ***Depolymerization of CCHO to dFCHO, seawater versus atmosphere.*** Free glucose, by far the most
734 prevailing monosaccharide among dFCHO in seawater, ranged between 0.6 and 51 $\mu\text{g L}^{-1}$ during the
735 PS106 cruise in the bulk and the SML (Zeppenfeld et al., 2019a). Thus, dFCHO/CHO ratios, meaning the
736 contribution of sugar monomers to all marine carbohydrates measured in this study, varied between
737 1–14% with an average of $5\pm 3\%$. Conversely, 86–99% (mean: 95 ± 3) of carbohydrates in the bulk and
738 SML of ocean seawater and melt ponds were incorporated into an oligo- or polysaccharidic structure.
739 CCHO can be hydrolyzed to dFCHO either in an acidic environment or enzymatically by heterotrophic
740 bacteria (Arnosti, 2000; Panagiotopoulos and Sempéré, 2005). Seawater from the Arctic Ocean is
741 slightly alkaline with reported pH values between 7.98 and 8.49 (Rérolle et al., 2016; Tynan et al.,
742 2016), while the pH of melt pond water has been observed to be more variable from mildly acidic (6.1)
743 to more alkaline (10.8) (Bates et al., 2014). In agreement with previous findings, the oceanic surface
744 seawater (pH: 7.98–8.66), including the samples from the MIZ, ice-free ocean and open
745 leads/polynyas, and the melt pond samples (pH: 7.26–8.62) were slightly alkaline in this study.
746 Consequently, it is more plausible that the depolymerization of CCHO in seawater can be ascribed to
747 bacterial activities rather than acid hydrolysis. Since dFCHO are readily resorbed by heterotrophic
748 bacteria with high turnover rates (Ittekkot et al., 1981; Kirchman et al., 2001), concentrations of these
749 monosaccharides are rather low in seawater.



750 In contrast, in aerosol particles, higher $dFCHO/CHO$ ratios up to 35% occurred in some selected
751 samples, which is much higher than in seawater, suggesting that CCHO might be depolymerized in the
752 atmosphere. SSA particles are known to significantly acidify within minutes after their release due to
753 the uptake of acidic gases, atmospheric aging reactions with sulfuric dioxide and water loss (Angle et
754 al., 2021). In this context, the surface-to-volume ratio determines the efficiency of the acidification
755 effect, which means that it is most pronounced for submicron SSA particles with reported pH values
756 of 1.5–2.6 within a few minutes in a tank study (Angle et al., 2021), and less pronounced for
757 supermicron SSA particles or cloud droplets (Angle et al., 2022). Consequently, it is conceivable that
758 an acid hydrolysis of $CCHO_{aer}$ to monomeric $dFCHO_{aer}$ occurs at the surface or within the bulk of SSA
759 aerosol particles leading to quick atmospheric aging. However, due to analytical constraints, such as
760 the limits of detections (LODs) of the methodology, the $dFCHO$ in size-resolved aerosol particles could
761 not be detected in all samples and the data availability is not strong enough to draw more conclusions
762 for aerosol particles.

763 In fog, where LODs did not represent an issue due to the high concentrations, $dFCHO/CHO$ ratios higher
764 than to seawater occurred (1–60%, mean: $27 \pm 16\%$) as well. The monosaccharide composition of
765 $dFCHO_{fog}$ was dominated by glucose, arabinose, fructose and xylose with small contributions from
766 glucosamine, galactose, mannose, rhamnose and fucose. Consequently, the monosaccharide
767 composition of $dFCHO_{fog}$ was quite similar to $CCHO_{fog}$, just with the difference that fructose was
768 detected in $dFCHO_{fog}$, but not in $CCHO_{fog}$, which is due to the low stability of fructose towards the
769 analytical preparation procedure for the analysis of CCHO (Panagiotopoulos and Sempéré, 2005) and
770 should, hence, not find further considerations. In this study, pH values of fog water ranged between
771 5.7 and 6.8, which is 1–2 magnitudes more acidic than in seawater. Polysaccharides are known to
772 depolymerize due to acid hydrolysis, especially at elevated temperatures. The pH-stability can be
773 largely variable among the different polysaccharides; however, we are not aware of studies that have
774 shown such fast depolymerizations, in the sense of time scales relevant for atmospheric lifetime of
775 aerosol particles, at such mildly acid conditions and low temperatures as those of the Arctic
776 atmosphere. Furthermore, there was no significant correlation between the pH and the $dFCHO/CHO$
777 of these cloud samples. Consequently, there are no indications that the majority of CCHO was
778 hydrolyzed inside the cloud droplets, however it might be conceivable that hydrolysis had readily
779 occurred within the non-activated SSA particle where pH values were much lower.

780 Besides an acid hydrolysis induced by quick atmospheric acidification of SSA particles, atmospheric
781 radicals, such as OH (Trueblood et al., 2019), or photolytic cleavages of glycosidic bonds (Kubota et al.,
782 1976) could have contributed to the degradation of atmospheric CCHO to monomeric $dFCHO$ in SSA
783 and marine fog. For these processes, however, still hardly any systematic lab studies have been



784 conducted for the plurality of marine polysaccharides, which makes a classification of the meaning of
785 these processes difficult. A preferred sea-air transfer of *d*FCCHO over CCHO to explain this observation
786 seems unlikely based on the missing enrichment of neutral *d*FCCHO in contrast to the high EF_{aer} of CCHO
787 shown in tank studies (Hasenecz et al., 2019, 2020). Finally, a microbial depolymerization of CCHO by
788 extracellular enzymes in fog cannot be entirely ruled out considering that the activity of some
789 polysaccharide-degrading enzymes, such as α - and β -glucosidase, have been found to accelerate in
790 seawater with increasing acidity (Piontek et al., 2010). However, this finding was conducted for a pH
791 range only 0.3 pH units lower than the typical pH of seawater and it is not sure, if this finding can be
792 transferred to the more acid conditions in aerosol particles and fog water.

793 ***Several aging processes in the atmosphere.*** We observed significant changes between the chemical
794 composition of marine carbohydrates in the surface seawater, including the bulk and SML, and
795 atmospheric carbohydrates, including aerosol particles and fog. Based on the changing
796 monosaccharide composition pattern of CCHO with selective degradation and formation of specific
797 monosaccharides within CCHO, we conclude microbial or enzymatic activities within the aerosol
798 particles of fog droplets. Furthermore, the increasing contribution of *d*FCCHO to the total carbohydrate
799 pool in fog and aerosol particles might be attributed to a hydrolytic cleavage of the glycosidic linkages
800 between monosaccharide units within the oligo- and polysaccharides after a quick atmospheric
801 acidification of SSA particles. Consequently, atmospheric carbohydrates experience quick atmospheric
802 aging, potentially due to both biological and abiotic processes, after their release from the ocean.
803 Possibly, this could affect the CCN and INP properties of marine carbohydrates and hence the
804 formation and properties of clouds.



805 **3.6 Perspective assessment of CCHO via bio-optical parameters**

806 The absorption of phytoplankton (a_{ph}) and CDOM (a_{CDOM}) are bio-optical parameters providing
807 additional information about the chemical and microbiological history of the water masses within the
808 particulate and dissolved phase, respectively. They can be measured on discrete water samples and
809 can also be assessed as products from satellites (Lefering et al., 2017; Matsuoka et al., 2012, 2013;
810 Röttgers et al., 2016). Here we tested, if a_{ph} or CDOM parameters correlate with CCHO in seawater to
811 potentially enable the remote-sensing approximation of marine CCHO in seawater and potentially in
812 the atmosphere.

813 **Good assessment of CCHO in seawater via a_{ph440} .** a_{ph440} derived from the phytoplankton absorption
814 spectrum is directly related to the biomarker TChl- a indicating phytoplankton biomass (Bricaud et al.,
815 2004; Phongphattarawat, 2016). The advantage of using a_{ph440} over pigment data, including TChl- a
816 from full high-performance liquid chromatography (HPLC) analysis (e.g. Barlow et al., 1997; Taylor et
817 al., 2011), is the lower need of sample volume for the analysis. This allows the determination of values
818 in the SML samples as well (Zäncker et al., 2017), which are laborious to collect and therefore limited
819 in availability. In this study, a_{ph440} strongly correlated with $pCCHO$ ($R=0.90$, $p<0.001$) in bulk and SML
820 samples (Figure SI 4) showing a direct link with fresh phytoplankton biomass production. A similar link
821 has been described before for TChl- a and $pCCHO$ in the photic layer of the Ross Sea (Fabiano et al.,
822 1993), in the ocean west of the Antarctic peninsula (Zeppenfeld et al., 2021a) and between TChl- a and
823 the particulate form of laminarin, an algal polysaccharide, in Arctic and Atlantic water samples (Becker
824 et al., 2020). $dCCHO$ showed a good, but weaker correlation with a_{ph440} ($R=0.66$, $p<0.001$) than
825 $pCCHO$. This finding supports the assumption that $pCCHO$ are rather freshly produced by local
826 autotrophs, while the link between $dCCHO$ with their primary production was already contorted by
827 subsequent transformation processes resulting in a more recalcitrant, long-lived mix of
828 macromolecules (Goldberg et al., 2011; Hansell, 2013; Keene et al., 2017). Nevertheless, CCHO, the
829 sum from $dCCHO$ and $pCCHO$, showed a high correlation with a_{ph440} ($R=0.84$, $p<0.001$) leading to the
830 conclusion that this bio-optical parameter derived from the $a_{ph}(\lambda)$ spectrum is suitable to assess the
831 total amount of CCHO in the surface seawater of the different sea-ice related sea surface
832 compartments of the Arctic.

833 **Good assessment of CCHO in seawater via $a_{CDOM350}$.** In this study, high correlations were observed
834 between $dCCHO$ and $a_{CDOM350}$ ($R=0.66$, $p<0.001$, Figure SI 5a), and weaker correlations between
835 $dCCHO$ and $a_{CDOM443}$ ($R=0.53$, $p<0.001$, Figure SI 5b). The better correlation at $\lambda=350$ nm compared to
836 443 nm can be explained by the fact that a_{CDOM} exponentially decreases with wavelength. While
837 absorption by CDOM is higher at $\lambda=350$ nm, it is much closer to the method detection limit at $\lambda=443$ nm



838 and is therefore more error-prone. However, with current satellite products only a_{CDOM} at 440 nm can
839 be retrieved.

840 Previous studies reported strong correlations between $a_{\text{CDOM}350}$ and dissolved organic carbon (DOC)
841 in Arctic seawater (Gonçalves-Araujo et al., 2015; Spencer et al., 2009; Stedmon et al., 2011; Walker
842 et al., 2013). Consequently, it is conceivable that $d\text{CCHO}$, an important constituent of DOC, shows good
843 correlations as well. Surprisingly, the correlation between CCHO (sum of $d\text{CCHO}$ and $p\text{CCHO}$) and
844 $a_{\text{CDOM}350}$ was strongest ($R=0.85$, $p<0.001$, [Figure SI 5c](#)), indicating that CDOM retrieval from high-
845 resolution satellite data could allow a good approximation of CCHO in Arctic seawater.



846 **4. Summary and Atmospheric Implications**

847 We studied the sea-air transfer of marine carbohydrates from field samples collected in the Arctic
848 during the PS106 campaign from May to July 2017. Large differences of absolute CCHO concentrations
849 and SML enrichments were observed among the different sea-ice related sea surface compartments
850 (leads/polynyas within the pack ice, ice-free ocean, MIZ, melt ponds). CCHO_{aer} were detected in the
851 sub- and supermicron aerosol particles with indications for primary emissions from the sea through
852 bubble bursting, though the correlations with the SSA tracer Na⁺ and wind speed were possibly
853 reduced due to the presence of sea ice influencing the wind-induced SSA emission mechanisms.
854 Atmospheric CCHO concentrations in fog strongly exceeded those of the aerosol particles, which might
855 be due to a phenomenon called fog scavenging and partly the comparability of the different sampling
856 approaches for fog and size-resolved aerosol particles. A large enrichment for CCHO in aerosol and fog
857 relative to seawater was observed, the extend of which varied on the type of sea-ice related sea
858 surface compartment assumed as the oceanic source. We observed a subsequent atmospheric aging
859 of CCHO in the atmosphere, both in aerosol particles and fog, noticed by the selective loss and
860 formation of certain monosaccharide units within CCHO suggesting selective enzymatic/microbial
861 activities, and a depolymerization of CCHO to *d*FCHO, most measurable in fog water and likely due to
862 abiotic degradation, e.g. acid hydrolysis. CCHO correlated well with bio-optical parameters, such as
863 a_{ph440} from phytoplankton absorption and $a_{CDOM350}$. These parameters can be measured via remote
864 sensing and may allow the retrieval of CCHO from satellite data, which potentially will enable an
865 accurate modelling of atmospheric CCHO concentrations as soon as all emission and atmospheric aging
866 processes are sufficiently understood. In a nutshell, this study shows that the Arctic is a complex
867 environment, where the diversity of sea-ice related sea surface compartments needs to be considered
868 as primary sources of marine CCHO or other organic compounds, and where these molecules can be
869 transformed after their primary sea-air transfer by biological and abiotic processes in the atmosphere.

870 Marine carbohydrates are assumed to impact cloud properties by acting as CCN and INP (Leck et al.,
871 2013; Orellana et al., 2011; van Pinxteren et al., 2022). Studying the chemical identity of those
872 atmospheric nucleation particles, their emission mechanisms and their transformation due to
873 atmospheric aging can strongly improve the understanding of the cloud formation in the Arctic, cloud
874 microphysical properties, the radiation budget, cryosphere-ocean-atmosphere interactions and
875 eventually feedback mechanisms in the frame of Arctic amplification. It can be assumed that within
876 the warming Arctic, where sea ice extent is continuously shrinking, the MIZ area will expand (Strong
877 and Rigor, 2013) and the number of biologically-active melt ponds will increase during the summer
878 season in the next years. These new MIZ regions and melt ponds could potentially produce more
879 marine carbohydrates than the ice-free ocean or open leads within the pack ice leading to enhanced



880 CCN and INP populations in the Arctic atmosphere serving as a still not well-explored feedback
881 mechanism within Arctic amplification.

882 **Data availability.** All data will be made available on the public repository PANGAEA.

883 **Author contribution.** SZ wrote the manuscript with contributions from MvP, MH, MZ, AB and HH. SZ,
884 MvP and MH collected the field samples during the PS106 campaign. SZ performed the laboratory
885 carbohydrate analysis and statistical evaluation. MZ and AB assessed the bio-optical parameters. All
886 co-authors proofread and commented the manuscript.

887 **Competing interests.** The authors declare that they have no conflict of interest.

888 **Acknowledgements.** We gratefully acknowledge the funding by the Deutsche Forschungsgemeinschaft
889 (DFG, German Research Foundation, Projektnummer 268020496–TRR 172) within the Transregional
890 Collaborative Research Center “Arctic Amplification: Climate Relevant Atmospheric and SurfaCe
891 Processes, and Feedback Mechanisms (AC)³”. This research has been supported by the DFG SPP 1158,
892 grant number 424326801 by enabling the access to melt pond data. We thank Andreas Macke and
893 Hauke Flores, chief scientists for the RV *Polarstern* cruises PS106.1 and PS106.2 (expedition grant
894 number AWI_PS106_00), and the captain and the crew of RV *Polarstern* for their support during the
895 expedition from May to July 2017. We thank Andrea Haudek and Hartmut Haudek for the development
896 and construction of the conditioning tube and the wind control system connected to the Berner
897 impactor. We thank Anett Dietze, Susanne Fuchs and Anke Rödger for the mass, inorganic ion and
898 OC/EC measurements. We acknowledge René Rabe and Sonja Wiegmann for supporting the
899 preparation of PS106 chemical equipment and optical instrumentation, respectively, and Yangyang Liu
900 for introducing the optical measurement procedure before PS106.

901 **Financial support.** This research has been supported by the Deutsche Forschungsgemeinschaft (DFG,
902 German Research Foundation, Projektnummer 268020496–TRR 172) within the Transregional
903 Collaborative Research Center “Arctic Amplification: Climate Relevant Atmospheric and SurfaCe
904 Processes, and Feedback Mechanisms (AC)³” in subprojects B04 and C03.

905 List of abbreviations

906	a_{CDOM}	absorption coefficient by colored dissolved organic carbon
907	aer	aerosol particles
908	a_{NAP}	absorption coefficient by non-algal particles
909	ANOVA	Analysis of Variance
910	a_p	absorption coefficient by total particles
911	a_{ph}	absorption coefficient by phytoplankton
912	Ara	arabinose
913	atmos	atmospheric concentrations
914	C-CCHO	carbon contained within the combined carbohydrate
915	CCHO	combined carbohydrates
916	CCN	cloud condensation nuclei



917	CDOM	colored dissolved organic matter
918	CHO	carbohydrates
919	<i>d</i> CCHO	dissolved combined carbohydrates
920	<i>d</i> FCHO	dissolved free carbohydrates
921	EF	enrichment factor
922	EPS	exopolymeric substances
923	ERDDAP	Environmental Research Division's Data Access Program
924	FAA	free amino acids
925	Fru	fructose
926	Fuc	fuco
927	Gal	galactose
928	GalN	galactosamine
929	GalAc	galacturonic acid
930	Glc	glucose
931	GlcAc	glucuronic acid
932	GlcN	glucosamine
933	HPAEC-PAD	high-performance anion-exchange chromatography with pulsed amperometric detection
934	HPLC	high-performance liquid chromatography
935	INP	ice nucleating particles
936	LWCC	liquid waveguide capillary cell
937	Man	mannose
938	MIZ	marginal ice zone
939	MurAc	muramic acid
940	Na ⁺	sodium ion
941	NOAA	National Oceanic and Atmospheric Administration
942	OC	organic carbon
943	OM	organic matter
944	PAB	particulate absorption
945	<i>p</i> CCHO	particulate combined carbohydrates
946	PM	particulate matter
947	Rha	rhamnose
948	SML	sea surface microlayer
949	SSA	sea spray aerosol
950	sub	submicron
951	super	supermicron
952	TChl- <i>a</i>	total chlorophyll <i>a</i>
953	TEP	transparent exopolymer particles
954	QFT-ICAM	quantitative filtration technique with an integrative-cavity absorption meter setup
955	Xyl	xylose



956 References

- 957 Alderkamp, A.-C., Buma, A. G. J., and van Rijssel, M.: The carbohydrates of Phaeocystis and their degradation in the microbial
958 food web, *Biogeochemistry*, 83, 99–118, <https://doi.org/10.1007/s10533-007-9078-2>, 2007.
- 959 Aller, J. Y., Kuznetsova, M. R., Jahns, C. J., and Kemp, P. F.: The sea surface microlayer as a source of viral and bacterial
960 enrichment in marine aerosols, *Journal of Aerosol Science*, 36, 801–812, <https://doi.org/10.1016/j.jaerosci.2004.10.012>,
961 2005.
- 962 Aller, J. Y., Radway, J. C., Kilhau, W. P., Bothe, D. W., Wilson, T. W., Vaillancourt, R. D., Quinn, P. K., Coffman, D. J., Murray,
963 B. J., and Knopf, D. A.: Size-resolved characterization of the polysaccharidic and proteinaceous components of sea spray
964 aerosol, *Atmospheric Environment*, 154, 331–347, <https://doi.org/10.1016/j.atmosenv.2017.01.053>, 2017.
- 965 Álvarez, E., Losa, S. N., Bracher, A., Thoms, S., and Völker, C.: Phytoplankton Light Absorption Impacted by Photoprotective
966 Carotenoids in a Global Ocean Spectrally-Resolved Biogeochemistry Model, *Journal of Advances in Modeling Earth Systems*,
967 14, e2022MS003126, <https://doi.org/10.1029/2022MS003126>, 2022.
- 968 Amon, R. M. W., Fitznar, H.-P., and Benner, R.: Linkages among the bioreactivity, chemical composition, and diagenetic state
969 of marine dissolved organic matter, *Limnology and Oceanography*, 46, 287–297, 2001.
- 970 Angle, K., Grassian, V. H., and Ault, A. P.: The rapid acidification of sea spray aerosols, *Physics today*, 75,
971 <https://doi.org/10.1063/PT.3.4926>, 2022.
- 972 Angle, K. J., Crocker, D. R., Simpson, R. M. C., Mayer, K. J., Garofalo, L. A., Moore, A. N., Garcia, S. L. M., Or, V. W., Srinivasan,
973 S., Farhan, M., Sauer, J. S., Lee, C., Pothier, M. A., Farmer, D. K., Martz, T. R., Bertram, T. H., Cappa, C. D., Prather, K. A., and
974 Grassian, V. H.: Acidity across the interface from the ocean surface to sea spray aerosol, *PNAS*, 118,
975 <https://doi.org/10.1073/pnas.2018397118>, 2021.
- 976 Arnosti, C.: Substrate specificity in polysaccharide hydrolysis: Contrasts between bottom water and sediments, *Limnology
977 and Oceanography*, 45, 1112–1119, <https://doi.org/10.4319/lo.2000.45.5.1112>, 2000.
- 978 Aslam, S. N., Michel, C., Niemi, A., and Underwood, G. J. C.: Patterns and drivers of carbohydrate budgets in ice algal
979 assemblages from first year Arctic sea ice, *Limnology and Oceanography*, 61, 919–937, <https://doi.org/10.1002/lno.10260>,
980 2016.
- 981 Azetsu-Scott, K. and Passow, U.: Ascending marine particles: Significance of transparent exopolymer particles (TEP) in the
982 upper ocean, *Limnology and Oceanography*, 49, 741–748, <https://doi.org/10.4319/lo.2004.49.3.0741>, 2004.
- 983 Barlow, R., Cummings, D., and Gibb, S.: Improved resolution of mono- and divinyl chlorophylls a and b and zeaxanthin and
984 lutein in phytoplankton extracts using reverse phase C-8 HPLC, *Marine Ecology Progress Series*, 161, 303–307,
985 <https://doi.org/10.3354/meps161303>, 1997.
- 986 Barthel, S., Tegen, I., and Wolke, R.: Do new sea spray aerosol source functions improve the results of a regional aerosol
987 model?, *Atmospheric Environment*, 198, 265–278, <https://doi.org/10.1016/j.atmosenv.2018.10.016>, 2019.
- 988 Bates, N. R., Garley, R., Frey, K. E., Shake, K. L., and Mathis, J. T.: Sea-ice melt CO₂-carbonate chemistry in the western Arctic
989 Ocean: meltwater contributions to air–sea CO₂ gas exchange, mixed-layer properties and rates of net community production
990 under sea ice, *Biogeosciences*, 11, 6769–6789, <https://doi.org/10.5194/bg-11-6769-2014>, 2014.
- 991 Becker, S., Tebben, J., Coffinet, S., Wiltshire, K., Iversen, M. H., Harder, T., Hinrichs, K.-U., and Hehemann, J.-H.: Laminarin is
992 a major molecule in the marine carbon cycle, *PNAS*, 117, 6599–6607, <https://doi.org/10.1073/pnas.1917001117>, 2020.
- 993 Benner, R. and Kaiser, K.: Abundance of amino sugars and peptidoglycan in marine particulate and dissolved organic matter,
994 *Limnology and Oceanography*, 48, 118–128, <https://doi.org/10.4319/lo.2003.48.1.0118>, 2003.
- 995 Bigg, E. K. and Leck, C.: The composition of fragments of bubbles bursting at the ocean surface, *Journal of Geophysical
996 Research: Atmospheres*, 113, <https://doi.org/10.1029/2007JD009078>, 2008.
- 997 Bikerman, J. J.: *Foams*, Springer Science & Business Media, 344 pp., 2013.
- 998 Bozem, H., Hoor, P., Kunkel, D., Köllner, F., Schneider, J., Herber, A., Schulz, H., Leaitch, W. R., Aliabadi, A. A., Willis, M. D.,
999 Burkart, J., and Abbatt, J. P. D.: Characterization of transport regimes and the polar dome during Arctic spring and summer
1000 using in situ aircraft measurements, *Atmospheric Chemistry and Physics*, 19, 15049–15071, [https://doi.org/10.5194/acp-19-
1001 15049-2019](https://doi.org/10.5194/acp-19-15049-2019), 2019.
- 1002 Bricaud, A., Claustre, H., Ras, J., and Oubelkheir, K.: Natural variability of phytoplanktonic absorption in oceanic waters:
1003 Influence of the size structure of algal populations, *Journal of Geophysical Research: Oceans*, 109,
1004 <https://doi.org/10.1029/2004JC002419>, 2004.
- 1005 Burrows, S. M., Ogunro, O., Frossard, A., Russell, L. M., Rasch, P. J., and Elliott, S.: A Physically Based Framework for Modelling
1006 the Organic Fractionation of Sea Spray Aerosol from Bubble Film Langmuir Equilibria, *Atmospheric Chemistry and Physics*,
1007 14(24):13601–13629, <https://doi.org/10.5194/acp-14-13601-2014>, 2014.



- 1008 Burrows, S. M., Gobrogge, E., Fu, L., Link, K., Elliott, S. M., Wang, H., and Walker, R.: OCEANFILMS-2: Representing
1009 coadsorption of saccharides in marine films and potential impacts on modeled marine aerosol chemistry, *Geophysical*
1010 *Research Letters*, 43, 8306–8313, <https://doi.org/10.1002/2016GL069070>, 2016.
- 1011 Callaghan, A. H., Deane, G. B., Stokes, M. D., and Ward, B.: Observed variation in the decay time of oceanic whitecap foam,
1012 *Journal of Geophysical Research: Oceans*, 117, <https://doi.org/10.1029/2012JC008147>, 2012.
- 1013 Casillo, A., Lanzetta, R., Parrilli, M., and Corsaro, M. M.: Exopolysaccharides from Marine and Marine Extremophilic Bacteria:
1014 Structures, Properties, Ecological Roles and Applications, *Marine Drugs*, 16, 69, <https://doi.org/10.3390/md16020069>, 2018.
- 1015 Chen, Q., Mirrieles, J. A., Thanekar, S., Loeb, N. A., Kirpes, R. M., Upchurch, L. M., Barget, A. J., Lata, N. N., Raso, A. R. W.,
1016 McNamara, S. M., China, S., Quinn, P. K., Ault, A. P., Kennedy, A., Shepson, P. B., Fuentes, J. D., and Pratt, K. A.: Atmospheric
1017 particle abundance and sea salt aerosol observations in the springtime Arctic: a focus on blowing snow and leads,
1018 *Atmospheric Chemistry and Physics*, 22, 15263–15285, <https://doi.org/10.5194/acp-22-15263-2022>, 2022.
- 1019 Chi, J. W., Li, W. J., Zhang, D. Z., Zhang, J. C., Lin, Y. T., Shen, X. J., Sun, J. Y., Chen, J. M., Zhang, X. Y., Zhang, Y. M., and Wang,
1020 W. X.: Sea salt aerosols as a reactive surface for inorganic and organic acidic gases in the Arctic troposphere, *Atmospheric*
1021 *Chemistry and Physics*, 15, 11341–11353, <https://doi.org/10.5194/acp-15-11341-2015>, 2015.
- 1022 Creamean, J. M., Barry, K., Hill, T. C. J., Hume, C., DeMott, P. J., Shupe, M. D., Dahlke, S., Willmes, S., Schmale, J., Beck, I.,
1023 Hoppe, C. J. M., Fong, A., Chamberlain, E., Bowman, J., Scharien, R., and Persson, O.: Annual cycle observations of aerosols
1024 capable of ice formation in central Arctic clouds, *Nat Commun*, 13, 3537, <https://doi.org/10.1038/s41467-022-31182-x>, 2022.
- 1025 Cunliffe, M., Engel, A., Frka, S., Gašparović, B., Guitart, C., Murrell, J. C., Salter, M., Stolle, C., Upstill-Goddard, R., and Wurl,
1026 O.: Sea surface microlayers: A unified physicochemical and biological perspective of the air–ocean interface, *Progress in*
1027 *Oceanography*, 109, 104–116, <https://doi.org/10.1016/j.pocean.2012.08.004>, 2013.
- 1028 Delort, A.-M., Vaïtilingom, M., Amato, P., Sancelme, M., Parazols, M., Mailhot, G., Laj, P., and Deguillaume, L.: A short
1029 overview of the microbial population in clouds: Potential roles in atmospheric chemistry and nucleation processes,
1030 *Atmospheric Research*, 98, 249–260, <https://doi.org/10.1016/j.atmosres.2010.07.004>, 2010.
- 1031 DeMott, P. J., Hill, T. C. J., McCluskey, C. S., Prather, K. A., Collins, D. B., Sullivan, R. C., Ruppel, M. J., Mason, R. H., Irish, V. E.,
1032 Lee, T., Hwang, C. Y., Rhee, T. S., Snider, J. R., McMeeking, G. R., Dhaniyala, S., Lewis, E. R., Wentzell, J. J. B., Abbatt, J., Lee,
1033 C., Sultana, C. M., Ault, A. P., Axson, J. L., Martinez, M. D., Venero, I., Santos-Figueroa, G., Stokes, M. D., Deane, G. B., Mayol-
1034 Bracero, O. L., Grassian, V. H., Bertram, T. H., Bertram, A. K., Moffett, B. F., and Franc, G. D.: Sea spray aerosol as a unique
1035 source of ice nucleating particles, *PNAS*, 113, 5797–5803, <https://doi.org/10.1073/pnas.1514034112>, 2016.
- 1036 Demoz, B. B., Collett, J. L., and Daube, B. C.: On the Caltech Active Strand Cloudwater Collectors, *Atmospheric Research*, 41,
1037 47–62, [https://doi.org/10.1016/0169-8095\(95\)00044-5](https://doi.org/10.1016/0169-8095(95)00044-5), 1996.
- 1038 Dominutti, P. A., Renard, P., Vaïtilingom, M., Bianco, A., Baray, J.-L., Borbon, A., Bourianne, T., Burnet, F., Colomb, A., Delort,
1039 A.-M., Duflot, V., Houdier, S., Jaffrezo, J.-L., Joly, M., Lerembouire, M., Metzger, J.-M., Pichon, J.-M., Ribeiro, M., Rocco, M.,
1040 Tulet, P., Vella, A., Leriche, M., and Deguillaume, L.: Insights into tropical cloud chemistry in Réunion (Indian Ocean): results
1041 from the BIO-MAÏDO campaign, *Atmospheric Chemistry and Physics*, 22, 505–533, <https://doi.org/10.5194/acp-22-505-2022>,
1042 2022.
- 1043 Engbrodt, R.: Biogeochemistry of dissolved carbohydrates in the Arctic, *Berichte zur Polar-und Meeresforschung (Reports on*
1044 *Polar and Marine Research)*, 396, 106pp, 2001.
- 1045 Engel, A. and Händel, N.: A novel protocol for determining the concentration and composition of sugars in particulate and in
1046 high molecular weight dissolved organic matter (HMW-DOM) in seawater, *Marine Chemistry*, 127, 180–191,
1047 <https://doi.org/10.1016/j.marchem.2011.09.004>, 2011.
- 1048 Engel, A., Bange, H. W., Cunliffe, M., Burrows, S. M., Friedrichs, G., Galgani, L., Herrmann, H., Hertkorn, N., Johnson, M., Liss,
1049 P. S., Quinn, P. K., Schartau, M., Soloviev, A., Stolle, C., Upstill-Goddard, R. C., van Pinxteren, M., and Zäncker, B.: The Ocean’s
1050 Vital Skin: Toward an Integrated Understanding of the Sea Surface Microlayer, *Front. Mar. Sci.*, 4, 165,
1051 <https://doi.org/10.3389/fmars.2017.00165>, 2017.
- 1052 Ervens, B. and Amato, P.: The global impact of bacterial processes on carbon mass, *Atmospheric Chemistry & Physics*, 20,
1053 1777–1794, <https://doi.org/10.5194/acp-20-1777-2020>, 2020.
- 1054 Fabiano, M., Povero, P., and Danovaro, R.: Distribution and composition of particulate organic matter in the Ross Sea
1055 (Antarctica), *Polar Biol*, 13, 525–533, <https://doi.org/10.1007/BF00236394>, 1993.
- 1056 Facchini, M. C., Rinaldi, M., Decesari, S., Carbone, C., Finessi, E., Mircea, M., Fuzzi, S., Ceburnis, D., Flanagan, R., Nilsson, E. D.,
1057 Leeuw, G. de, Martino, M., Woeltjen, J., and O’Dowd, C. D.: Primary submicron marine aerosol dominated by insoluble organic
1058 colloids and aggregates, *Geophysical Research Letters*, 35, <https://doi.org/10.1029/2008GL034210>, 2008.
- 1059 Galgani, L., Piontek, J., and Engel, A.: Biopolymers form a gelatinous microlayer at the air–sea interface when Arctic sea ice
1060 melts, *Scientific Reports*, 6, 29465, <https://doi.org/10.1038/srep29465>, 2016.



- 1061 Gantt, B., Meskhidze, N., Facchini, M. C., Rinaldi, M., Ceburnis, D., and O'Dowd, C. D.: Wind speed dependent size-resolved
1062 parameterization for the organic mass fraction of sea spray aerosol, *Atmospheric Chemistry and Physics*, 11, 8777–8790,
1063 <https://doi.org/10.5194/acp-11-8777-2011>, 2011.
- 1064 Gao, Q., Leck, C., Rauschenberg, C., and Matrai, P. A.: On the chemical dynamics of extracellular polysaccharides in the high
1065 Arctic surface microlayer, *Ocean Science*, 8, 401–418, 2012.
- 1066 Gilardoni, S., Massoli, P., Giulianelli, L., Rinaldi, M., Paglione, M., Pollini, F., Lanconelli, C., Poluzzi, V., Carbone, S., Hillamo, R.,
1067 Russell, L. M., Facchini, M. C., and Fuzzi, S.: Fog scavenging of organic and inorganic aerosol in the Po Valley, *Atmospheric
1068 Chemistry and Physics*, 14, 6967–6981, <https://doi.org/10.5194/acp-14-6967-2014>, 2014.
- 1069 Goldberg, S. J., Carlson, C. A., Brzezinski, M., Nelson, N. B., and Siegel, D. A.: Systematic removal of neutral sugars within
1070 dissolved organic matter across ocean basins, *Geophysical Research Letters*, 38, <https://doi.org/10.1029/2011GL048620>,
1071 2011.
- 1072 Gonçalves-Araujo, R., Stedmon, C. A., Heim, B., Dubinenkov, I., Kraberg, A., Moiseev, D., and Bracher, A.: From Fresh to Marine
1073 Waters: Characterization and Fate of Dissolved Organic Matter in the Lena River Delta Region, Siberia, *Frontiers in Marine
1074 Science*, 2, 2015.
- 1075 Grythe, H., Ström, J., Krejci, R., Quinn, P., and Stohl, A.: A review of sea-spray aerosol source functions using a large global set
1076 of sea salt aerosol concentration measurements, *Atmospheric Chemistry and Physics*, 14, 1277–1297,
1077 <https://doi.org/10.5194/acp-14-1277-2014>, 2014.
- 1078 Haddrell, A. E. and Thomas, R. J.: Aerobiology: Experimental Considerations, Observations, and Future Tools, *Appl. Environ.
1079 Microbiol.*, 83, <https://doi.org/10.1128/AEM.00809-17>, 2017.
- 1080 Hansell, D. A.: Recalcitrant Dissolved Organic Carbon Fractions, *Annual Review of Marine Science*, 5, 421–445,
1081 <https://doi.org/10.1146/annurev-marine-120710-100757>, 2013.
- 1082 Hara, K., Yamagata, S., Yamanouchi, T., Sato, K., Herber, A., Iwasaka, Y., Nagatani, M., and Nakata, H.: Mixing states of
1083 individual aerosol particles in spring Arctic troposphere during ASTAR 2000 campaign, *Journal of Geophysical Research:
1084 Atmospheres*, 108, <https://doi.org/10.1029/2002JD002513>, 2003.
- 1085 Hartmann, M., Gong, X., Kecorius, S., van Pinxteren, M., Vogl, T., Welti, A., Wex, H., Zeppenfeld, S., Herrmann, H.,
1086 Wiedensohler, A., and Stratmann, F.: Terrestrial or marine – indications towards the origin of ice-nucleating particles during
1087 melt season in the European Arctic up to 83.7° N, *Atmospheric Chemistry and Physics*, 21, 11613–11636,
1088 <https://doi.org/10.5194/acp-21-11613-2021>, 2021.
- 1089 Hasenecz, E., Jayarathne, T., Pendergraft, M. A., Santander, M. V., Mayer, K. J., Sauer, J., Lee, C., Gibson, W. S., Kruse, S. M.,
1090 Malfatti, F., Prather, K. A., and Stone, E. A.: Marine bacteria affect saccharide enrichment in sea spray aerosol during a
1091 phytoplankton bloom, *ACS Earth Space Chem.*, 4, 1638–1649, <https://doi.org/10.1021/acsearthspacechem.0c00167>, 2020.
- 1092 Hasenecz, E. S., Kaluarachchi, C. P., Lee, H. D., Tivanski, A. V., and Stone, E. A.: Saccharide Transfer to Sea Spray Aerosol
1093 Enhanced by Surface Activity, Calcium, and Protein Interactions, *ACS Earth Space Chem.*, 3, 2539–2548,
1094 <https://doi.org/10.1021/acsearthspacechem.9b00197>, 2019.
- 1095 Held, A., Brooks, I. M., Leck, C., and Tjernström, M.: On the potential contribution of open lead particle emissions to the
1096 central Arctic aerosol concentration, *Atmospheric Chemistry and Physics*, 11, 3093–3105, [https://doi.org/10.5194/acp-11-
1097 3093-2011](https://doi.org/10.5194/acp-11-3093-2011), 2011.
- 1098 Hoffman, E. J. and Duce, R. A.: Factors influencing the organic carbon content of marine aerosols: A laboratory study, *Journal
1099 of Geophysical Research (1896-1977)*, 81, 3667–3670, <https://doi.org/10.1029/JC081i021p03667>, 1976.
- 1100 Istomina, L.: Retrieval of Sea Ice Surface Melt Using OLCI Data Onboard Sentinel-3, 2020, C017-07, 2020.
- 1101 Ittekkot, V., Brockmann, U., Michaelis, W., and Degens, E. T.: Dissolved free and combined carbohydrates during a
1102 phytoplankton bloom in the northern North Sea, *Marine Ecology Progress Series*, 4, 299–305, 1981.
- 1103 Karl, M., Leck, C., Rad, F. M., Bäcklund, A., Lopez-Aparicio, S., and Heintzenberg, J.: New insights in sources of the sub-
1104 micrometre aerosol at Mt. Zeppelin observatory (Spitsbergen) in the year 2015, *Tellus B: Chemical and Physical Meteorology*,
1105 71, 1613143, <https://doi.org/10.1080/16000889.2019.1613143>, 2019.
- 1106 Kecorius, S., Vogl, T., Paasonen, P., Lampilahti, J., Rothenberg, D., Wex, H., Zeppenfeld, S., van Pinxteren, M., Hartmann, M.,
1107 Henning, S., Gong, X., Welti, A., Kulmala, M., Stratmann, F., Herrmann, H., and Wiedensohler, A.: New particle formation and
1108 its effect on cloud condensation nuclei abundance in the summer Arctic: a case study in the Fram Strait and Barents Sea,
1109 *Atmospheric Chemistry and Physics*, 19, 14339–14364, <https://doi.org/10.5194/acp-19-14339-2019>, 2019.
- 1110 Keene, W. C., Long, M. S., Reid, J. S., Frossard, A. A., Kieber, D. J., Maben, J. R., Russell, L. M., Kinsey, J. D., Quinn, P. K., and
1111 Bates, T. S.: Factors That Modulate Properties of Primary Marine Aerosol Generated From Ambient Seawater on Ships at Sea,
1112 *Journal of Geophysical Research: Atmospheres*, 122, 11,961-11,990, <https://doi.org/10.1002/2017JD026872>, 2017.



- 1113 Kirchman, D. L., Meon, B., Ducklow, H. W., Carlson, C. A., Hansell, D. A., and Steward, G. F.: Glucose fluxes and concentrations
1114 of dissolved combined neutral sugars (polysaccharides) in the Ross Sea and Polar Front Zone, Antarctica, *Deep Sea Research*
1115 *Part II: Topical Studies in Oceanography*, 48, 4179–4197, [https://doi.org/10.1016/S0967-0645\(01\)00085-6](https://doi.org/10.1016/S0967-0645(01)00085-6), 2001.
- 1116 Krembs, C. and Deming, J. W.: The role of exopolymers in microbial adaptation to sea ice, in: *Psychrophiles: from biodiversity*
1117 *to biotechnology*, Springer, 247–264, 2008.
- 1118 Krembs, C., Eicken, H., Junge, K., and Deming, J. W.: High concentrations of exopolymeric substances in Arctic winter sea ice:
1119 implications for the polar ocean carbon cycle and cryoprotection of diatoms, *Deep Sea Research Part I: Oceanographic*
1120 *Research Papers*, 49, 2163–2181, [https://doi.org/10.1016/S0967-0637\(02\)00122-X](https://doi.org/10.1016/S0967-0637(02)00122-X), 2002.
- 1121 Kubota, H., Ogiwara, Y., and Matsuzaki, K.: Photo-Induced Formation of Peroxide in Saccharides and Related Compounds,
1122 *Polymer Journal*, 8, 557–563, <https://doi.org/10.1295/polymj.8.557>, 1976.
- 1123 Lawler, M. J., Saltzman, E. S., Karlsson, L., Zieger, P., Salter, M., Baccarini, A., Schmale, J., and Leck, C.: New Insights Into the
1124 Composition and Origins of Ultrafine Aerosol in the Summertime High Arctic, *Geophysical Research Letters*, 48,
1125 e2021GL094395, <https://doi.org/10.1029/2021GL094395>, 2021.
- 1126 Leck, C.: Chemical composition and sources of the high Arctic aerosol relevant for cloud formation, *Journal of Geophysical*
1127 *Research*, 107, <https://doi.org/10.1029/2001JD001463>, 2002.
- 1128 Leck, C., Gao, Q., Mashayekhy Rad, F., and Nilsson, U.: Size-resolved atmospheric particulate polysaccharides in the high
1129 summer Arctic, *Atmospheric Chemistry and Physics*, 13, 12573–12588, <https://doi.org/10.5194/acp-13-12573-2013>, 2013.
- 1130 Lefering, I., Röttgers, R., Utschig, C., and McKee, D.: Uncertainty budgets for liquid waveguide CDOM absorption
1131 measurements, *Appl. Opt.*, AO, 56, 6357–6366, <https://doi.org/10.1364/AO.56.006357>, 2017.
- 1132 Liu, Y., Röttgers, R., Ramírez-Pérez, M., Dinter, T., Steinmetz, F., Nöthig, E.-M., Hellmann, S., Wiegmann, S., and Bracher, A.:
1133 Underway spectrophotometry in the Fram Strait (European Arctic Ocean): a highly resolved chlorophyll a data source for
1134 complementing satellite ocean color, *Opt. Express*, OE, 26, A678–A696, <https://doi.org/10.1364/OE.26.00A678>, 2018.
- 1135 Macke, A. and Flores, H.: The Expeditions PS106/1 and 2 of the Research Vessel POLARSTERN to the Arctic Ocean in 2017,
1136 Bremerhaven, Germany, 171 pp., https://doi.org/10.2312/BzPM_0719_2018, 2018.
- 1137 Malfatti, F., Lee, C., Tinta, T., Pendergraft, M. A., Celussi, M., Zhou, Y., Sultana, C. M., Rotter, A., Axson, J. L., Collins, D. B.,
1138 Santander, M. V., Anides Morales, A. L., Aluwihare, L. I., Riemer, N., Grassian, V. H., Azam, F., and Prather, K. A.: Detection of
1139 Active Microbial Enzymes in Nascent Sea Spray Aerosol: Implications for Atmospheric Chemistry and Climate, *Environ. Sci.*
1140 *Technol. Lett.*, 6, 171–177, <https://doi.org/10.1021/acs.estlett.8b00699>, 2019.
- 1141 Mari, X., Passow, U., Migon, C., Burd, A. B., and Legendre, L.: Transparent exopolymer particles: Effects on carbon cycling in
1142 the ocean, *Progress in Oceanography*, 151, 13–37, <https://doi.org/10.1016/j.pocean.2016.11.002>, 2017.
- 1143 Marks, R., Kruczalak, K., Jankowska, K., and Michalska, M.: Bacteria and fungi in air over the Gulf of Gdańsk and Baltic sea,
1144 *Journal of Aerosol Science*, 32, 237–250, [https://doi.org/10.1016/S0021-8502\(00\)00064-1](https://doi.org/10.1016/S0021-8502(00)00064-1), 2001.
- 1145 Matsuoka, A., Bricaud, A., Benner, R., Para, J., Sempéré, R., Prieur, L., Bélanger, S., and Babin, M.: Tracing the transport of
1146 colored dissolved organic matter in water masses of the Southern Beaufort Sea: relationship with hydrographic
1147 characteristics, *Biogeosciences*, 9, 925–940, <https://doi.org/10.5194/bg-9-925-2012>, 2012.
- 1148 Matsuoka, A., Hooker, S. B., Bricaud, A., Gentili, B., and Babin, M.: Estimating absorption coefficients of colored dissolved
1149 organic matter (CDOM) using a semi-analytical algorithm for southern Beaufort Sea waters: application to deriving
1150 concentrations of dissolved organic carbon from space, *Biogeosciences*, 10, 917–927, [https://doi.org/10.5194/bg-10-917-](https://doi.org/10.5194/bg-10-917-2013)
1151 [2013](https://doi.org/10.5194/bg-10-917-2013), 2013.
- 1152 Matulová, M., Husárová, S., Capek, P., Sancelme, M., and Delort, A.-M.: Biotransformation of Various Saccharides and
1153 Production of Exopolymeric Substances by Cloud-Borne *Bacillus* sp. 3B6, *Environ. Sci. Technol.*, 48, 14238–14247,
1154 <https://doi.org/10.1021/es501350s>, 2014.
- 1155 Mayol, E., Arrieta, J. M., Jiménez, M. A., Martínez-Asensio, A., Garcías-Bonet, N., Dachs, J., González-Gaya, B., Royer, S.-J.,
1156 Benítez-Barrios, V. M., Fraile-Nuez, E., and Duarte, C. M.: Long-range transport of airborne microbes over the global tropical
1157 and subtropical ocean, *Nature Communications*, 8, 1–9, <https://doi.org/10.1038/s41467-017-00110-9>, 2017.
- 1158 McCarthy, M., Hedges, J., and Benner, R.: Major biochemical composition of dissolved high molecular weight organic matter
1159 in seawater, *Marine Chemistry*, 55, 281–297, [https://doi.org/10.1016/S0304-4203\(96\)00041-2](https://doi.org/10.1016/S0304-4203(96)00041-2), 1996.
- 1160 McCluskey, C. S., Hill, T. C. J., Humphries, R. S., Rauker, A. M., Moreau, S., Strutton, P. G., Chambers, S. D., Williams, A. G.,
1161 McRobert, I., Ward, J., Keywood, M. D., Harnwell, J., Ponsonby, W., Loh, Z. M., Krummel, P. B., Protat, A., Kreidenweis, S. M.,
1162 and DeMott, P. J.: Observations of Ice Nucleating Particles Over Southern Ocean Waters, *Geophysical Research Letters*, 45,
1163 11,989–11,997, <https://doi.org/10.1029/2018GL079981>, 2018.
- 1164 Mimura, T. and Romano, J. C.: Muramic Acid measurements for bacterial investigations in marine environments by high-
1165 pressure liquid chromatography, *Appl. Environ. Microbiol.*, 50, 229–237, <https://doi.org/10.1128/AEM.50.2.229-237.1985>,
1166 1985.



- 1167 Mühlenbruch, M., Grossart, H.-P., Eigemann, F., and Voss, M.: Mini-review: Phytoplankton-derived polysaccharides in the
1168 marine environment and their interactions with heterotrophic bacteria, *Environmental Microbiology*, 20, 2671–2685,
1169 <https://doi.org/10.1111/1462-2920.14302>, 2018.
- 1170 Müller, K., Lehmann, S., Pinxteren, D. van, Gnauk, T., Niedermeier, N., Wiedensohler, A., and Herrmann, H.: Particle
1171 characterization at the Cape Verde atmospheric observatory during the 2007 RHaMBLe intensive, *Atmospheric Chemistry
1172 and Physics*, 10, 2709–2721, <https://doi.org/10.5194/acp-10-2709-2010>, 2010.
- 1173 Norris, S. J., Brooks, I. M., de Leeuw, G., Sirevaag, A., Leck, C., Brooks, B. J., Birch, C. E., and Tjernström, M.: Measurements of
1174 bubble size spectra within leads in the Arctic summer pack ice, *Ocean Science*, 7, 129–139, [https://doi.org/10.5194/os-7-129-
1175 2011](https://doi.org/10.5194/os-7-129-2011), 2011.
- 1176 Notz, D. and Worster, M. G.: Desalination processes of sea ice revisited, *Journal of Geophysical Research: Oceans*, 114,
1177 <https://doi.org/10.1029/2008JC004885>, 2009.
- 1178 Obernosterer, I., Catala, P., Lami, R., Caparros, J., Ras, J., Bricaud, A., Christine, D., Van Wambeke, F., and Lebaron, P.:
1179 Biochemical characteristics and bacterial community structure of the sea surface microlayer in the South Pacific Ocean,
1180 *Biogeosciences*, 5, 693–705, 2008.
- 1181 O’Dowd, C. D., Facchini, M. C., Cavalli, F., Ceburnis, D., Mircea, M., Decesari, S., Fuzzi, S., Yoon, Y. J., and Putaud, J.-P.:
1182 Biogenically driven organic contribution to marine aerosol, *Nature*, 431, 676–680, <https://doi.org/10.1038/nature02959>,
1183 2004.
- 1184 Orellana, M. V., Matrai, P. A., Leck, C., Rauschenberg, C. D., Lee, A. M., and Coz, E.: Marine microgels as a source of cloud
1185 condensation nuclei in the high Arctic, *PNAS*, 108, 13612–13617, <https://doi.org/10.1073/pnas.1102457108>, 2011.
- 1186 Panagiotopoulos, C. and Sempéré, R.: Analytical methods for the determination of sugars in marine samples: A historical
1187 perspective and future directions, *Limnology and Oceanography: Methods*, 3, 419–454,
1188 <https://doi.org/10.4319/lom.2005.3.419>, 2005.
- 1189 Papakonstantinou-Presvelou, I., Sourdeval, O., and Quaas, J.: Strong Ocean/Sea-Ice Contrasts Observed in Satellite-Derived
1190 Ice Crystal Number Concentrations in Arctic Ice Boundary-Layer Clouds, *Geophysical Research Letters*, 49, e2022GL098207,
1191 <https://doi.org/10.1029/2022GL098207>, 2022.
- 1192 Passow, U.: Transparent exopolymer particles (TEP) in aquatic environments, *Progress in Oceanography*, 55, 287–333,
1193 [https://doi.org/10.1016/S0079-6611\(02\)00138-6](https://doi.org/10.1016/S0079-6611(02)00138-6), 2002.
- 1194 Penner, J. E., Andreae, M. O., Annegarn, H., Barrie, L., Feichter, J., Hegg, D., Jayaraman, A., Leaitch, R., Murphy, D., Nganga,
1195 J., and Pitari, G.: Aerosols, their Direct and Indirect Effects, *Climate Change 2001: The Scientific Basis. Contribution of Working
1196 Group I to the Third Assessment Report of the Intergovernmental Panel on Climate Change*, 289–348, 2001.
- 1197 Phongphattarawat, S.: Variability in pigment composition and bio-optical characteristics of phytoplankton populations in the
1198 Atlantic basin, <http://purl.org/dc/dcmitype/Text>, University of Oxford, 2016.
- 1199 van Pinxteren, M., Müller, C., Iinuma, Y., Stolle, C., and Herrmann, H.: Chemical Characterization of Dissolved Organic
1200 Compounds from Coastal Sea Surface Microlayers (Baltic Sea, Germany), *Environmental Science & Technology*, 46, 10455–
1201 10462, <https://doi.org/10.1021/es204492b>, 2012.
- 1202 van Pinxteren, M., Barthel, S., Fomba, K. W., Müller, K., Von Tümpling, W., and Herrmann, H.: The influence of environmental
1203 drivers on the enrichment of organic carbon in the sea surface microlayer and in submicron aerosol particles – measurements
1204 from the Atlantic Ocean, *Elem Sci Anth*, 5, <https://doi.org/10.1525/elementa.225>, 2017.
- 1205 van Pinxteren, M., Robinson, T.-B., Zeppenfeld, S., Gong, X., Bahlmann, E., Fomba, K. W., Triesch, N., Stratmann, F., Wurl, O.,
1206 Engel, A., Wex, H., and Herrmann, H.: High number concentrations of transparent exopolymer particles in ambient aerosol
1207 particles and cloud water – a case study at the tropical Atlantic Ocean, *Atmospheric Chemistry and Physics*, 22, 5725–5742,
1208 <https://doi.org/10.5194/acp-22-5725-2022>, 2022.
- 1209 van Pinxteren, M., Zeppenfeld, S., Fomba, K. W., Triesch, N., Frka, S., and Herrmann, H.: Amino acids, carbohydrates, and
1210 lipids in the tropical oligotrophic Atlantic Ocean: sea-to-air transfer and atmospheric in situ formation, *Atmospheric Chemistry
1211 and Physics*, 23, 6571–6590, <https://doi.org/10.5194/acp-23-6571-2023>, 2023.
- 1212 Piontek, J., Lunau, M., Händel, N., Borchard, C., Wurst, M., and Engel, A.: Acidification increases microbial polysaccharide
1213 degradation in the ocean, *Biogeosciences*, 7, 1615–1624, <https://doi.org/10.5194/bg-7-1615-2010>, 2010.
- 1214 Porter, G. C. E., Adams, M. P., Brooks, I. M., Ickes, L., Karlsson, L., Leck, C., Salter, M. E., Schmale, J., Siegel, K., Sikora, S. N. F.,
1215 Tarn, M. D., Vüllers, J., Wernli, H., Zieger, P., Zinke, J., and Murray, B. J.: Highly Active Ice-Nucleating Particles at the Summer
1216 North Pole, *Journal of Geophysical Research: Atmospheres*, 127, e2021JD036059, <https://doi.org/10.1029/2021JD036059>,
1217 2022.
- 1218 Prather, K. A., Bertram, T. H., Grassian, V. H., Deane, G. B., Stokes, M. D., DeMott, P. J., Aluwihare, L. I., Palenik, B. P., Azam,
1219 F., Seinfeld, J. H., Moffet, R. C., Molina, M. J., Cappa, C. D., Geiger, F. M., Roberts, G. C., Russell, L. M., Ault, A. P., Baltrusaitis,
1220 J., Collins, D. B., Corrigan, C. E., Cuadra-Rodriguez, L. A., Ebben, C. J., Forestieri, S. D., Guasco, T. L., Hersey, S. P., Kim, M. J.,



- 1221 Lambert, W. F., Modini, R. L., Mui, W., Pedler, B. E., Ruppel, M. J., Ryder, O. S., Schoepp, N. G., Sullivan, R. C., and Zhao, D.:
1222 Bringing the ocean into the laboratory to probe the chemical complexity of sea spray aerosol, *PNAS*, 110, 7550–7555,
1223 <https://doi.org/10.1073/pnas.1300262110>, 2013.
- 1224 Qin, G., Zhu, L., Chen, X., Wang, P. G., and Zhang, Y.: Structural characterization and ecological roles of a novel
1225 exopolysaccharide from the deep-sea psychrotolerant bacterium *Pseudoalteromonas* sp. SM9913, *Microbiology*, 153, 1566–
1226 1572, <https://doi.org/10.1099/mic.0.2006/003327-0>, 2007.
- 1227 Quinn, P. K., Collins, D. B., Grassian, V. H., Prather, K. A., and Bates, T. S.: Chemistry and Related Properties of Freshly Emitted
1228 Sea Spray Aerosol, *Chemical Reviews*, 115, 4383–4399, <https://doi.org/10.1021/cr500713g>, 2015.
- 1229 Rastelli, E., Corinaldesi, C., Dell'Anno, A., Lo Martire, M., Greco, S., Cristina Facchini, M., Rinaldi, M., O'Dowd, C., Ceburnis, D.,
1230 and Danovaro, R.: Transfer of labile organic matter and microbes from the ocean surface to the marine aerosol: an
1231 experimental approach, *Scientific Reports*, 7, 1–10, <https://doi.org/10.1038/s41598-017-10563-z>, 2017.
- 1232 Rérolle, V., Ruiz-Pino, D., Rafizadeh, M., Loucaides, S., Papadimitriou, S., Mowlem, M., and Chen, J.: Measuring pH in the
1233 Arctic Ocean: Colorimetric method or SeaFET?, *Methods in Oceanography*, 17, 32–49,
1234 <https://doi.org/10.1016/j.mio.2016.05.006>, 2016.
- 1235 Robinson, T.-B., Wurl, O., Bahlmann, E., Jürgens, K., and Stolle, C.: Rising bubbles enhance the gelatinous nature of the air–
1236 sea interface, *Limnology and Oceanography*, 64, 2358–2372, <https://doi.org/10.1002/lno.11188>, 2019.
- 1237 Rolph, R. J., Feltham, D. L., and Schröder, D.: Changes of the Arctic marginal ice zone during the satellite era, *The Cryosphere*,
1238 14, 1971–1984, <https://doi.org/10.5194/tc-14-1971-2020>, 2020.
- 1239 Röttgers, R., McKee, D., and Utschig, C.: Temperature and salinity correction coefficients for light absorption by water in the
1240 visible to infrared spectral region, *Opt. Express*, OE, 22, 25093–25108, <https://doi.org/10.1364/OE.22.025093>, 2014.
- 1241 Röttgers, R., Doxaran, D., and Dupouy, C.: Quantitative filter technique measurements of spectral light absorption by aquatic
1242 particles using a portable integrating cavity absorption meter (QFT-ICAM), *Opt. Express*, OE, 24, A1–A20,
1243 <https://doi.org/10.1364/OE.24.0000A1>, 2016.
- 1244 Russell, L. M., Hawkins, L. N., Frossard, A. A., Quinn, P. K., and Bates, T. S.: Carbohydrate-like composition of submicron
1245 atmospheric particles and their production from ocean bubble bursting, *Proc. Natl. Acad. Sci. U.S.A.*, 107, 6652–6657,
1246 <https://doi.org/10.1073/pnas.0908905107>, 2010.
- 1247 Šantl-Temkiv, T., Gosewinkel, U., Starnawski, P., Lever, M., and Finster, K.: Aeolian dispersal of bacteria in southwest
1248 Greenland: their sources, abundance, diversity and physiological states, *FEMS Microbiol Ecol*, 94,
1249 <https://doi.org/10.1093/femsec/fiy031>, 2018.
- 1250 Šantl-Temkiv, T., Sikoparija, B., Maki, T., Carotenuto, F., Amato, P., Yao, M., Morris, C. E., Schnell, R., Jaenicke, R., Pöhlker, C.,
1251 DeMott, P. J., Hill, T. C. J., and Huffman, J. A.: Bioaerosol field measurements: Challenges and perspectives in outdoor studies,
1252 *Aerosol Science and Technology*, 54, 520–546, <https://doi.org/10.1080/02786826.2019.1676395>, 2020.
- 1253 Schiffer, J. M., Mael, L. E., Prather, K. A., Amaro, R. E., and Grassian, V. H.: Sea Spray Aerosol: Where Marine Biology Meets
1254 Atmospheric Chemistry, *ACS Cent. Sci.*, 4, 1617–1623, <https://doi.org/10.1021/acscentsci.8b00674>, 2018.
- 1255 Schill, S. R., Burrows, S. M., Hasenecz, E. S., Stone, E. A., and Bertram, T. H.: The Impact of Divalent Cations on the Enrichment
1256 of Soluble Saccharides in Primary Sea Spray Aerosol, *Atmosphere*, 9, 476, <https://doi.org/10.3390/atmos9120476>, 2018.
- 1257 Schmale, J., Zieger, P., and Ekman, A. M. L.: Aerosols in current and future Arctic climate, *Nature Climate Change*, 11, 95–105,
1258 <https://doi.org/10.1038/s41558-020-00969-5>, 2021.
- 1259 Schmithüsen, H.: Continuous meteorological surface measurement during POLARSTERN cruise PS106/1 (ARK-XXXI/1.1),
1260 <https://doi.org/10.1594/PANGAEA.886302>, 2018.
- 1261 Schmithüsen, H.: Continuous meteorological surface measurement during POLARSTERN cruise PS106/2 (ARK-XXXI/1.2),
1262 <https://doi.org/10.1594/PANGAEA.901179>, 2019.
- 1263 Schmitt-Kopplin, P., Liger-Belair, G., Koch, B. P., Flerus, R., Kattner, G., Harir, M., Kanawati, B., Lucio, M., Tziotis, D., Hertkorn,
1264 N., and Gebefügi, I.: Dissolved organic matter in sea spray: a transfer study from marine surface water to aerosols,
1265 *Biogeosciences*, 9, 1571–1582, 2012.
- 1266 Sellegri, K., O'Dowd, C. D., Yoon, Y. J., Jennings, S. G., and Leeuw, G. de: Surfactants and submicron sea spray generation,
1267 *Journal of Geophysical Research: Atmospheres*, 111, <https://doi.org/10.1029/2005JD006658>, 2006.
- 1268 Spencer, R. G. M., Aiken, G. R., Butler, K. D., Dornblaser, M. M., Striegl, R. G., and Hernes, P. J.: Utilizing chromophoric dissolved
1269 organic matter measurements to derive export and reactivity of dissolved organic carbon exported to the Arctic Ocean: A
1270 case study of the Yukon River, Alaska, *Geophysical Research Letters*, 36, <https://doi.org/10.1029/2008GL036831>, 2009.
- 1271 Stedmon, C. A., Amon, R. M. W., Rinehart, A. J., and Walker, S. A.: The supply and characteristics of colored dissolved organic
1272 matter (CDOM) in the Arctic Ocean: Pan Arctic trends and differences, *Marine Chemistry*, 124, 108–118,
1273 <https://doi.org/10.1016/j.marchem.2010.12.007>, 2011.



- 1274 Stein, A. F., Draxler, R. R., Rolph, G. D., Stunder, B. J. B., Cohen, M. D., and Ngan, F.: NOAA's HYSPLIT Atmospheric Transport
1275 and Dispersion Modeling System, *Bull. Amer. Meteor. Soc.*, 96, 2059–2077, <https://doi.org/10.1175/BAMS-D-14-00110.1>,
1276 2015.
- 1277 Stolle, C., Nagel, K., Labrenz, M., and Jürgens, K.: Succession of the sea-surface microlayer in the coastal Baltic Sea under
1278 natural and experimentally induced low-wind conditions, *Biogeosciences*, 7, 2975–2988, [https://doi.org/10.5194/bg-7-2975-](https://doi.org/10.5194/bg-7-2975-2010)
1279 2010, 2010.
- 1280 Strong, C. and Rigor, I. G.: Arctic marginal ice zone trending wider in summer and narrower in winter, *Geophysical Research*
1281 *Letters*, 40, 4864–4868, <https://doi.org/10.1002/grl.50928>, 2013.
- 1282 Sud, I. J. and Tyler, M. E.: Cell-Wall Composition and Osmotic Fragility of Selected Marine Bacteria, *Journal of Bacteriology*,
1283 87, 696–700, 1964.
- 1284 Suzuki, E. and Suzuki, R.: Variation of Storage Polysaccharides in Phototrophic Microorganisms, *Journal of Applied*
1285 *Glycoscience*, 60, 21–27, https://doi.org/10.5458/jag.jag.JAG-2012_016, 2013.
- 1286 Taylor, B. B., Torrecilla, E., Bernhardt, A., Taylor, M. H., Peeken, I., Röttgers, R., Piera, J., and Bracher, A.: Bio-optical provinces
1287 in the eastern Atlantic Ocean and their biogeographical relevance, 8, 7165–7219, <https://doi.org/10.5194/bg-d-8-7165-2011>,
1288 2011.
- 1289 Thomson, J.: Wave propagation in the marginal ice zone: connections and feedback mechanisms within the air–ice–ocean
1290 system, *Philosophical Transactions of the Royal Society A: Mathematical, Physical and Engineering Sciences*, 380, 20210251,
1291 <https://doi.org/10.1098/rsta.2021.0251>, 2022.
- 1292 Triesch, N., van Pinxteren, M., Engel, A., and Herrmann, H.: Concerted measurements of free amino acids at the Cabo Verde
1293 islands: high enrichments in submicron sea spray aerosol particles and cloud droplets, *Atmospheric Chemistry and Physics*,
1294 21, 163–181, <https://doi.org/10.5194/acp-21-163-2021>, 2021a.
- 1295 Triesch, N., van Pinxteren, M., Frka, S., Stolle, C., Spranger, T., Hoffmann, E. H., Gong, X., Wex, H., Schulz-Bull, D., Gašparović,
1296 B., and Herrmann, H.: Concerted measurements of lipids in seawater and on submicrometer aerosol particles at the Cabo
1297 Verde islands: biogenic sources, selective transfer and high enrichments, *Atmospheric Chemistry and Physics*, 21, 4267–4283,
1298 <https://doi.org/10.5194/acp-21-4267-2021>, 2021b.
- 1299 Triesch, N., van Pinxteren, M., Salter, M., Stolle, C., Pereira, R., Zieger, P., and Herrmann, H.: Sea Spray Aerosol Chamber Study
1300 on Selective Transfer and Enrichment of Free and Combined Amino Acids, *ACS Earth Space Chem.*, 5, 1564–1574,
1301 <https://doi.org/10.1021/acsearthspacechem.1c00080>, 2021c.
- 1302 Trueblood, J. V., Wang, X., Or, V. W., Alves, M. R., Santander, M. V., Prather, K. A., and Grassian, V. H.: The Old and the New:
1303 Aging of Sea Spray Aerosol and Formation of Secondary Marine Aerosol through OH Oxidation Reactions, *ACS Earth Space*
1304 *Chem.*, 3, 2307–2314, <https://doi.org/10.1021/acsearthspacechem.9b00087>, 2019.
- 1305 Tynan, E., Clarke, J. S., Humphreys, M. P., Ribas-Ribas, M., Esposito, M., Rérolle, V. M. C., Schlosser, C., Thorpe, S. E., Tyrrell,
1306 T., and Achterberg, E. P.: Physical and biogeochemical controls on the variability in surface pH and calcium carbonate
1307 saturation states in the Atlantic sectors of the Arctic and Southern Oceans, *Deep Sea Research Part II: Topical Studies in*
1308 *Oceanography*, 127, 7–27, <https://doi.org/10.1016/j.dsr2.2016.01.001>, 2016.
- 1309 Uetake, J., Hill, T. C. J., Moore, K. A., DeMott, P. J., Protat, A., and Kreidenweis, S. M.: Airborne bacteria confirm the pristine
1310 nature of the Southern Ocean boundary layer, *PNAS*, 117, 13275–13282, <https://doi.org/10.1073/pnas.2000134117>, 2020.
- 1311 Vaqué, D., Boras, J. A., Arrieta, J. M., Agustí, S., Duarte, C. M., and Sala, M. M.: Enhanced Viral Activity in the Surface Microlayer
1312 of the Arctic and Antarctic Oceans, *Microorganisms*, 9, 317, <https://doi.org/10.3390/microorganisms9020317>, 2021.
- 1313 Veron, F.: Ocean Spray, *Annual Review of Fluid Mechanics*, 47, 507–538, [https://doi.org/10.1146/annurev-fluid-010814-](https://doi.org/10.1146/annurev-fluid-010814-014651)
1314 014651, 2015.
- 1315 Walker, S. A., Amon, R. M. W., and Stedmon, C. A.: Variations in high-latitude riverine fluorescent dissolved organic matter:
1316 A comparison of large Arctic rivers, *Journal of Geophysical Research: Biogeosciences*, 118, 1689–1702,
1317 <https://doi.org/10.1002/2013JG002320>, 2013.
- 1318 Wang, X., Deane, G. B., Moore, K. A., Ryder, O. S., Stokes, M. D., Beall, C. M., Collins, D. B., Santander, M. V., Burrows, S. M.,
1319 Sultana, C. M., and Prather, K. A.: The role of jet and film drops in controlling the mixing state of submicron sea spray aerosol
1320 particles, *PNAS*, 114, 6978–6983, <https://doi.org/10.1073/pnas.1702420114>, 2017.
- 1321 Wendisch, M., Macke, A., Ehrlich, A., Lüpkes, C., Mech, M., Chechin, D., Dethloff, K., Barentos, C., Bozem, H., Brückner, M.,
1322 Clemen, H.-C., Crewell, S., Donth, T., Dupuy, R., Ebell, K., Egerer, U., Engelmann, R., Engler, C., Eppers, O., Gehrman, M.,
1323 Gong, X., Gottschalk, M., Gourbeyre, C., Griesche, H., Hartmann, J., Hartmann, M., Heinold, B., Herber, A., Herrmann, H.,
1324 Heygster, G., Hoor, P., Jafariserajehlou, S., Jäkel, E., Järvinen, E., Jourdan, O., Kästner, U., Kecorius, S., Knudsen, E. M., Köllner,
1325 F., Kretschmar, J., Lelli, L., Leroy, D., Maturilli, M., Mei, L., Mertes, S., Mioche, G., Neuber, R., Nicolaus, M., Nomokonova, T.,
1326 Notholt, J., Palm, M., van Pinxteren, M., Quaas, J., Richter, P., Ruiz-Donoso, E., Schäfer, M., Schmieder, K., Schnaiter, M.,
1327 Schneider, J., Schwarzenböck, A., Seifert, P., Shupe, M. D., Siebert, H., Spreen, G., Stapf, J., Stratmann, F., Vogl, T., Welti, A.,
1328 Wex, H., Wiedensohler, A., Zannata, M., and Zeppenfeld, S.: The Arctic Cloud Puzzle: Using ALOUD/PASCAL Multi-Platform



- 1329 Observations to Unravel the Role of Clouds and Aerosol Particles in Arctic Amplification, *Bull. Amer. Meteor. Soc.*,
1330 <https://doi.org/10.1175/BAMS-D-18-0072.1>, 2018.
- 1331 Wendisch, M., Brückner, M., Crewell, S., Ehrlich, A., Notholt, J., Lüpkes, C., Macke, A., Burrows, J. P., Rinke, A., Quaas, J.,
1332 Maturilli, M., Schemann, V., Shupe, M. D., Akansu, E. F., Barrientos-Velasco, C., Bärfuss, K., Blechschmidt, A.-M., Block, K.,
1333 Bougoudis, I., Bozem, H., Böckmann, C., Bracher, A., Bresson, H., Bretschneider, L., Buschmann, M., Chechin, D. G., Chylik, J.,
1334 Dahlke, S., Deneke, H., Dethloff, K., Donth, T., Dorn, W., Dupuy, R., Ebell, K., Egerer, U., Engelmann, R., Eppers, O., Gerdes, R.,
1335 Gierens, R., Gorodetskaya, I. V., Gottschalk, M., Griesche, H., Gryanik, V. M., Handorf, D., Harm-Altstädter, B., Hartmann, J.,
1336 Hartmann, M., Heinold, B., Herber, A., Herrmann, H., Heygster, G., Höschel, I., Hofmann, Z., Hölemann, J., Hünerbein, A.,
1337 Jafariserajehlou, S., Jäkel, E., Jacobi, C., Janout, M., Jansen, F., Jourdan, O., Jurányi, Z., Kalesse-Los, H., Kanzow, T., Käthner,
1338 R., Kliesch, L. L., Klingebiel, M., Knudsen, E. M., Kovács, T., Körtke, W., Krampe, D., Kretschmar, J., Kreyling, D., Kulla, B.,
1339 Kunkel, D., Lampert, A., Lauer, M., Lelli, L., Lerber, A. von, Linke, O., Löhnert, U., Lonardi, M., Losa, S. N., Losch, M., Maahn,
1340 M., Mech, M., Mei, L., Mertens, S., Metzner, E., Mewes, D., Michaelis, J., Mioche, G., Moser, M., Nakoudi, K., Neggers, R.,
1341 Neuber, R., Nomokonova, T., Oelker, J., Papakonstantinou-Prevelou, I., et al.: Atmospheric and Surface Processes, and
1342 Feedback Mechanisms Determining Arctic Amplification: A Review of First Results and Prospects of the (AC)3 Project, *Bulletin*
1343 *of the American Meteorological Society*, 104, E208–E242, <https://doi.org/10.1175/BAMS-D-21-0218.1>, 2023.
- 1344 Wietz, M., Wemheuer, B., Simon, H., Giebel, H.-A., Seibt, M. A., Daniel, R., Brinkhoff, T., and Simon, M.: Bacterial community
1345 dynamics during polysaccharide degradation at contrasting sites in the Southern and Atlantic Oceans, *Environ. Microbiol.*, 17,
1346 3822–3831, <https://doi.org/10.1111/1462-2920.12842>, 2015.
- 1347 Wilbourn, E. K., Thornton, D. C. O., Ott, C., Graff, J., Quinn, P. K., Bates, T. S., Betha, R., Russell, L. M., Behrenfeld, M. J., and
1348 Brooks, S. D.: Ice Nucleation by Marine Aerosols Over the North Atlantic Ocean in Late Spring, *Journal of Geophysical*
1349 *Research: Atmospheres*, 125, e2019JD030913, <https://doi.org/10.1029/2019JD030913>, 2020.
- 1350 Williams, P. M., Carlucci, A. F., Henrichs, S. M., Van Vleet, E. S., Horrigan, S. G., Reid, F. M. H., and Robertson, K. J.: Chemical
1351 and microbiological studies of sea-surface films in the Southern Gulf of California and off the West Coast of Baja California,
1352 *Marine Chemistry*, 19, 17–98, [https://doi.org/10.1016/0304-4203\(86\)90033-2](https://doi.org/10.1016/0304-4203(86)90033-2), 1986.
- 1353 Wurl, O., Miller, L., Röttgers, R., and Vagle, S.: The distribution and fate of surface-active substances in the sea-surface
1354 microlayer and water column, *Marine Chemistry*, 115, 1–9, <https://doi.org/10.1016/j.marchem.2009.04.007>, 2009.
- 1355 Wurl, O., Miller, L., and Vagle, S.: Production and fate of transparent exopolymer particles in the ocean, *Journal of Geophysical*
1356 *Research: Oceans*, 116, <https://doi.org/10.1029/2011JC007342>, 2011.
- 1357 Xu, M., Tsona Tchinda, N., Li, J., and Du, L.: Insoluble lipid film mediates transfer of soluble saccharides from the sea to the
1358 atmosphere: the role of hydrogen bonding, *Atmospheric Chemistry and Physics*, 23, 2235–2249, <https://doi.org/10.5194/acp-23-2235-2023>, 2023.
- 1360 Xu, W., Ovadnevaite, J., Fossum, K. N., Lin, C., Huang, R.-J., Ceburnis, D., and O’Dowd, C.: Sea spray as an obscured source for
1361 marine cloud nuclei, *Nat. Geosci.*, 15, 282–286, <https://doi.org/10.1038/s41561-022-00917-2>, 2022.
- 1362 Yang, X., Pyle, J. A., and Cox, R. A.: Sea salt aerosol production and bromine release: Role of snow on sea ice, *Geophysical*
1363 *Research Letters*, 35, <https://doi.org/10.1029/2008GL034536>, 2008.
- 1364 Zábóri, J., Matisāns, M., Krejci, R., Nilsson, E. D., and Ström, J.: Artificial primary marine aerosol production: a laboratory study
1365 with varying water temperature, salinity, and succinic acid concentration, *Atmospheric Chemistry and Physics*, 12, 10709–
1366 10724, <https://doi.org/10.5194/acp-12-10709-2012>, 2012.
- 1367 Zäncker, B., Bracher, A., Röttgers, R., and Engel, A.: Variations of the Organic Matter Composition in the Sea Surface
1368 Microlayer: A Comparison between Open Ocean, Coastal, and Upwelling Sites Off the Peruvian Coast, *Frontiers in*
1369 *Microbiology*, 8, 2369, <https://doi.org/10.3389/fmicb.2017.02369>, 2017.
- 1370 Zäncker, B., Cunliffe, M., and Engel, A.: Eukaryotic community composition in the sea surface microlayer across an east–west
1371 transect in the Mediterranean Sea, *Biogeosciences*, 18, 2107–2118, <https://doi.org/10.5194/bg-18-2107-2021>, 2021.
- 1372 Zeppenfeld, S., van Pinxteren, M., Hartmann, M., Bracher, A., Stratmann, F., and Herrmann, H.: Glucose as a Potential
1373 Chemical Marker for Ice Nucleating Activity in Arctic Seawater and Melt Pond Samples, *Environ. Sci. Technol.*, 53, 8747–8756,
1374 <https://doi.org/10.1021/acs.est.9b01469>, 2019a.
- 1375 Zeppenfeld, S., van Pinxteren, M., Hartmann, M., Bracher, A., Wiegmann, S., Stratmann, F., and Herrmann, H.: Glucose, T50
1376 and salinity in the surface microlayer and bulk water samples from the Arctic during POLARSTERN cruise PS106 (2017),
1377 <https://doi.org/10.1594/PANGAEA.899258>, 2019b.
- 1378 Zeppenfeld, S., van Pinxteren, M., Engel, A., and Herrmann, H.: A protocol for quantifying mono- and polysaccharides in
1379 seawater and related saline matrices by electro-dialysis (ED) – combined with HPAEC-PAD, *Ocean Science*, 16, 817–830,
1380 <https://doi.org/10.5194/os-16-817-2020>, 2020.
- 1381 Zeppenfeld, S., van Pinxteren, M., van Pinxteren, D., Wex, H., Berdalet, E., Vaqué, D., Dall’Osto, M., and Herrmann, H.: Aerosol
1382 Marine Primary Carbohydrates and Atmospheric Transformation in the Western Antarctic Peninsula, *ACS Earth Space Chem.*,
1383 5, 1032–1047, <https://doi.org/10.1021/acsearthspacechem.0c00351>, 2021a.



- 1384 Zeppenfeld, S., Fuchs, S., Rödger, S., Dietze, A., van Pinxteren, M., and Herrmann, H.: Marine carbohydrates and inorganic
1385 ions in size-resolved atmospheric particles collected over the Southern Ocean, <https://doi.org/10.1594/PANGAEA.927565>,
1386 2021b.
- 1387 Zinke, J., Salter, M. E., Leck, C., Lawler, M. J., Porter, G. C. E., Adams, M. P., Brooks, I. M., Murray, B. J., and Zieger, P.: The
1388 development of a miniaturised balloon-borne cloud water sampler and its first deployment in the high Arctic, *Tellus B:*
1389 *Chemical and Physical Meteorology*, 73, 1–12, <https://doi.org/10.1080/16000889.2021.1915614>, 2021.
- 1390